RESEARCH ARTICLE VOLCANICA

Origin and significance of volcanic garnet: A detailed petro-mineralogical study of the almandine-bearing andesite of Breziny (Central Slovakia Volcanic Field, Western Carpathians, central Europe)

Jacky Bouloton*
Université Clermont Auvergne, CNRS, IRD, OPGC, Laboratoire Magmas et Volcans, F-63000 Clermont-Ferrand, France.

Abstract

Almandine-rich garnets from a Neogene andesite of Slovakia can be divided into two main types. Garnet megacrysts are magmatic and form a chemically homogeneous group that contains, on average, about 5 wt% CaO and 4.5 wt% MgO as petrogenetically significant components. Garnets occurring in lithic fragments and garnets aggregated in garnetite lenses are characterised by Ca-poor cores (CaO $\leqslant$ 2 wt%) that testify for a two-step history and correspond respectively to inherited pre-anatectic and peritectic garnets. Available experimental data show that the composition of magmatic garnet megacrysts is compatible with a peritectic origin, through the fluid-absent melting of an immature metasedimentary protolith or a tonalitic gneiss. However, thermal evolution evidenced by zircons shielded in garnet rather suggests that garnet nucleated and grew by cooling of a hybrid magma pool, resulting from the complete mixing of crust- and mantle-derived melts.

Keywords: `Volcanic garnet; Crustal melting; Experimental petrology constraints; Cotectic vs. Peritectic; Central Slovakia Volcanic Field`

1 Introduction

Garnets are uncommon in volcanic rocks and evaluating their origin may provide critical information on open-system magma evolution at depth. The Neogene calc-alkaline series of the Carpatho-Pannonian region offers one of the largest collections of garnet-bearing volcanics in the world. The deep origin of this almandine garnet has been established for a long time. Petrographic studies [Brousse et al. 1972; Embey-Isztin et al. 1985] have shown that these garnets represent a high-pressure igneous phase, partly resorbed by reaction with its host liquid at shallower depths, rather than xenocrysts derived from disaggregated high-level country rocks. More recently, on the basis of Sr and Nd isotopic ratios of the garnet-bearing lavas combined with the oxygen isotope composition of bulk garnets, Harangi et al. [2001] proposed that garnet crystallised from M- or I-type magmas contaminated by a significant amount of lower-crustal metasedimentary material. Garnet would have crystallised at high pressures (7–12 kbar) and temperatures (800–940 °C), probably near the mantle-crust boundary zone [Harangi et al. 2001]. However, it has been proposed very recently [Rottier et al. 2019] that magmatic garnet in fact crystallised at "low" temperatures (down to ~750 °C) from an evolved, residual melt derived from fractionation of a primitive magma of mantle origin. This assumption, based in particular on the example of the Breziny andesitic dome, is at odds with former interpretations. Whatever the assumption about its precise origin, volcanic garnet in the Carpathians had been implicitly or explicitly described as an early-crystallising, near-liquidus phase [Brousse et al. 1972; Embey-Isztin et al. 1985; Harangi et al. 2001; Bouloton and Paquette 2014]. Moreover, oxygen isotope data strongly suggest that the crust, one way or another, was involved in garnet genesis [Harangi et al. 2001]. It is because of these inconsistencies that this petro-mineralogical study was undertaken.

The deep origin of volcanic almandine garnet is in accordance with the results of crystallisation experiments that suggest that magmatic garnet should be common at depth in silicic and intermediate melts [Green and Ringwood 1968; Green 1972; 1982; Carroll and Wyllie 1990; Green 1992]. On the other hand, it is well-known that peritectic garnet is a common by-product of most fluid-absent melting reactions at pressures corresponding to the lowermost crust [Thompson 1982; Le Breton and Thompson 1988; Vielzeuf and Holloway 1988; Vielzeuf and Montel 1994; Patiño Douce and Beard 1995; Stevens et al. 1997]. This leads to an open-system situation in which crustal- and mantle-derived melts may chemically and physically interact in the deep crust. Most of the current understanding of this melting, assimilation, storage, and homogenisation (MASH) zone [Hildreth and Moorbath 1988] is based on inter-

*Corresponding author: jacky.bouloton@free.fr

pretation of trace element and isotopic compositions, a cryptic process based on modelling supposed end-members with little control (if any) on the actual mineralogy of the crustal source. Thus, characterising the origin of volcanic garnet on a mineralogical and petrological basis should be a mandatory step in constraining magma evolution in the "deep crustal hot zone" [Annen et al. 2006], another name commonly used to designate the MASH zone. At a time when the importance of lower crustal processes in global dynamics of igneous systems is emphasised [Cashman et al. 2017], high-pressure volcanic garnets may *a priori* provide significant insights into petrogenetic processes hidden at depth.

High-pressure magmatic garnet has two possible origins: it may either nucleate and grow as a cotectic garnet from a cooling magma pool or crystallise as the solid peritectic product of an incongruent melting reaction at the site of anatexis, prior to being entrained upward. As melting appears as the easiest process accounting for dissolution and assimilation of metasedimentary material by mantle-derived magmas, this immediately raises the question of the possible peritectic nature of volcanic garnet. It is likely that peritectic garnet produced during the melting event, as well as pre-anatectic garnet inherited from the lower crustal source, may be preserved under favourable circumstances in the mixed magma. Thus, the focus of this study is to evaluate the ultimate origin of volcanic garnet by distinguishing xenocrystic, pre-anatectic, peritectic, and cotectic garnets.

2 Geological setting

2.1 Calc-alkaline volcanism of the Carpathians and its significance

The Carpathian volcanic arc is an arcuate belt of calc-alkaline volcanic complexes that extends more than 1500 km along the northern and eastern margin of the Pannonian Basin (Figure 1). It is composed mostly of andesites and dacites mainly erupted from the Middle Miocene and continuing through the Pliocene. The tectonic history of the area is complicated, and the relationship between the calc-alkaline volcanic activity and the geodynamic evolution has been widely debated in the past. In summary, the geological context implies a Miocene convergence and subduction event, followed by crustal extension related to the formation of the Pannonian basin. No volcanic activity clearly related to the pre-collisional subduction is recorded in the whole Carpatho-Pannonian area [Seghedi 2010] and subduction was only playing an indirect role, if any [Harangi et al. 2007]. It is now widely accepted that magmas in this area were generated above the downgoing slab during the back-arc extension period and, therefore, could be directly related to the main extensional phase of the Pannonian Basin [Lexa and Konečný 1998; Harangi et al. 2001].

The geochemical signature of these calc-alkaline magmas is complex, and their precise origin is debatable. According to Seghedi [2004], large-volume partial melts of a heterogeneous asthenospheric mantle source caused underplating and crustal anatexis, leading to mixing of mantle-derived calc-alkaline magmas with crustal melts. According to Harangi et al. [2007], calc-alkaline magmas were formed by melting of a metasomatised, enriched lithospheric mantle modified by addition of fluids and sediments and were contaminated by various crustal materials. More precisely, mixing of mafic magmas with silicic melts from metasedimentary lower crust would result in relatively Al-rich hybrid dacitic magmas from which almandine-rich garnet could crystallise at high pressure [Harangi et al. 2007]. In any case, melting of the lower crust is explicitly assumed and though garnet-bearing lavas are volumetrically minor; assessing the origin of garnet, therefore, represents a primary objective in order to delineate the effects of crustal assimilation versus source contamination (i.e. the addition of subducted sediment to the mantle source region).

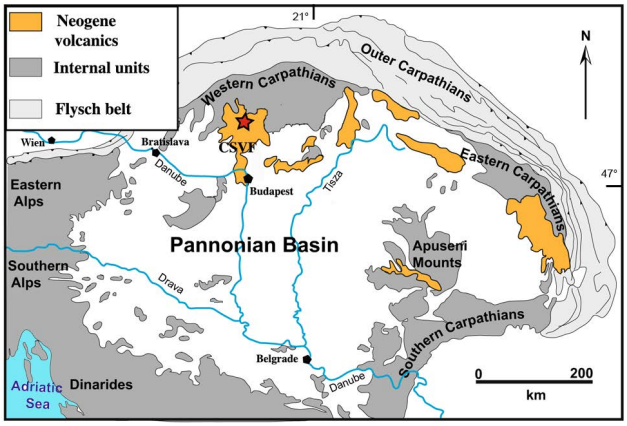

Figure 1: Simplified geological map of the Carpatho-Pannonian region, showing the distribution of the Neogene volcanic rocks (coloured) and the location of the andesitic dome near the village of Breziny (red star). CSVF = Central Slovakia Volcanic Field. Slightly modified after Didier et al. [2015].

2.2 Garnet-bearing volcanics

Almandine garnet is found along the entire Carpathian arc from Slovakia to Romania and occurs as discrete megacrysts in lavas from intermediate (andesitic) to acidic (rhyolitic) composition. Garnet-bearing volcanic rocks are most abundant in the West Carpathians [Harangi et al. 2001], but the highest garnet contents (up to 5 % volume) have been recorded in the eastern segment [Nitoi et al. 2002]. In the West Carpathians, calc-

alkaline activity began with widespread acid pyroclastic explosions and was followed in the largest volcanic area—the Central Slovakia Volcanic Field (CSVF)—by the formation of four mainly andesitic stratovolcanoes (Štiavnica, Javorie, Vtáčnik, and Pol'ana) located at the inner margin of the arc. Garnet is typically related to the first phase of this andesitic activity [Konečný et al. 1995] and is interpreted to be Badennian in age (15–16.4 Ma; [Seghedi 2010]; 15.0 ± 0.4 Ma, K-Ar age [Chernyshev et al. 2013]). These garnet-bearing andesites could be younger, as suggested by recent *in situ* laser ablation inductively coupled plasma mass spectrometry (LA-ICP-MS) U-Pb results (13.3 ± 0.1 Ma) obtained on zircons shielded in garnets [Bouloton and Paquette 2014].

The main mineralogical characteristics of these garnet-bearing lavas have been summarised by Harangi et al. [2001]. Plagioclase is the most common phenocryst coexisting with garnet. Hornblende and biotite also occur frequently, both phases coexisting in the most silicic andesites and the less silicic dacites. Biotite is absent from the andesites, whereas it is the only mafic mineral in the rhyodacites. According to Harangi et al. [2001], clinopyroxene has never been observed and orthopyroxene occurs sporadically. Importantly, mineral phases characteristic of many garnet-bearing S-type volcanic rocks worldwide, such as quartz, cordierite, and K-feldspar, are absent from the Carpathian garnet-bearing lavas [Harangi et al. 2001].

2.3 Breziny andesite

The andesitic dome of Breziny, located 5 km south of the city of Zvolen, is one of the well-known examples of garnet-bearing andesite in Slovakia. It forms part of the Neresnica formation, a discontinuous horizon present throughout the CSVF and that constitutes the lower unit of the Štiavnica stratovolcano. This formation is composed of scattered garnet-bearing andesitic extrusive domes, with related reworked breccias and epiclastic rocks [Konečný et al. 1995]. More precisely, the andesitic dome of Breziny—hereafter referred in this study as the Breziny andesite—is an extrusive dome of irregular elliptic section, elongated North–South, where the long axis is ~2500 m. The massive andesite of the core is rimmed by extrusive breccias of variable thickness (5–10 m) formed by disintegration of the andesite dome during its growth [Konečný et al. 1998a; b].

The studied garnet-bearing lava (SK8) was collected in a quarry located about 1 km NE of the village of Breziny. GPS coordinates of the quarry are 48° 31' 17" N, 019° 05' 57" E. A lot of samples were collected there, from which more than fifty thin-sections were prepared. This lava was specifically chosen for a comprehensive petrologic study for three reasons: 1) evidence of mingling of different batches of melt, examplified by the coexistence of several types of amphibole; 2) presence of high-grade garnet-bearing metasedimentary enclaves that could potentially be related to the genesis of the volcanic garnet megacrysts; 3) the ambiguous status of orthopyroxene, that is exceedingly rare as a phenocryst but forms frequent inclusions in garnet. Chemical composition of the Breziny garnet has been reported many times in the literature [Brousse et al. 1972; Fediukova 1975; Irving and Frey 1978; Harangi et al. 2001; Bouloton and Paquette 2014; Rottier et al. 2019]. However, the origin and significance of this phase are still debatable.

3 Objectives of the study and analytical techniques

3.1 Objectives

If trace elements and radiogenic isotopes actually testify for magma hybridisation, the real story of magma crystallisation is written in the texture of the rocks and the major element zonation of the main phases. For this reason, the approach adopted in this study combines textural information and characterisation of major element chemistry of minerals, independent of any trace element or isotopic consideration. Results from this classical petrographic investigation are then compared with currently available high pressure–high temperature (HP–HT) experimental data in order to propose a plausible scenario for garnet generation. Although some trace elements (e.g. HREE) are strongly fractionated in garnet, it is clear that they do not control the genesis of this phase. The compositional parameters that control garnet stability include Al-oversaturation and the Fe-Mg-Ca-Mn ratios. Accordingly, bearing in mind that a_{SiO_2}, a_{H_2O} and f_{O_2} are critical in phase equilibrium constraints of magmatic systems, it is assumed that major elements are sufficient to discuss the stability of volcanic garnet.

3.2 Terminology

Considering the existence of different and somewhat confusing vocabularies, I specify hereafter the terminology followed in this paper, mainly inspired from Hildreth and Wilson [2007] and Miller et al. [2007]. *Megacryst* is a purely descriptive term used to designate larger crystals in the lava whatever their origin. *Phenocrysts* are larger native crystals grown from a melt; depending on their genetic relation with their host, they may either correspond to *ortho-* or *antecrysts*. *Orthocryst* describes crystals that have crystallised from a magma with the bulk composition of their host, cognate crystals precipitated from a liquid whose residue was chilled to form the present-day groundmass. *Antecryst* refers to crystals that belong to the magmatic system that produced their host but did not directly crystallise from this host; they have grown in a discrete but

kindred melt, known or inferred to have been an earlier component of the magmatic system. *Xenocryst* is used for crystals that are clearly foreign to the rocks in which they occur; they are unrelated to the magma system and correspond to accidental inclusions scavenged by the magma from the wall-rocks at any level above the primary source region. Finally, *restite* refers to minerals derived from the source region of the magma and comprise two different types of minerals: 1) the remaining solid crystalline residue of partial melting, primary minerals present in the source rocks before melting and left in excess by the melting reaction, and 2) the solid products of the incongruent (mostly fluid-absent) melt-generating reactions (peritectic minerals). Residual solid material not involved in the melting reaction (refractory layers) should be defined as *resister* or *resistate*; together with primary minerals left over by the melting reaction, resister minerals represent a heritage from the source and may be designated as *pre-anatectic* phases.

3.3 Methods

Thorough petrographic observations are a prerequisite for identifying the phases that were in equilibrium with garnet and melt. This requires more specifically determining the relationships between garnet and hornblende phenocrysts. This is indeed the key argument to decide whether garnets grew from their present-day enclosing groundmass, as proposed by Harangi et al. [2001], or not. In this perspective, a combination of optical microscopy and back-scattered electron (BSE) imaging, electron-microprobe analysis (EMPA) of major elements and X-ray element mapping was used. Spot microprobe analyses were performed at Laboratoire Magmas et Volcans (LMV), Clermont Auvergne University (France), on a Cameca SX 100 four-spectrometer instrument. Run conditions for spot analyses were 15 kV accelerating voltage, 15 nA sample current and minimum probe diameter (beam size about 1 µm). Counting times were 10 s on the peak and 10 s on the background. Natural and synthetic minerals were used as standards and results are considered accurate to within 1–6 % relative. BSE images were either acquired with the Cameca microprobe or with the Scanning Electron Microscope JEOL JSM-5910 LV hosted at the LMV.

Particular attention has been paid to garnet zonation by analysing detailed traverses across the zoned crystals and creating X-ray element maps using the Cameca SX 100. Sample current was 15 nA and counting times 10 s for the profiles. For X-ray imaging, sample current was maintained between 965 and 1000 nA and counting time was 100 ms/pixel. The resolution of the X-ray images is 512 × 512 pixels. Four images were acquired simultaneously during sessions which lasted about 8 h. Ca, Mg, Mn, and Ti were principally studied. Additionally, a few Fe, P, and Y images were acquired, but these elements have been quickly left aside, as they did not provide significant additional information.

4 Petrology of the lava and its garnet-bearing enclaves

4.1 Chemical characteristics

Two samples of lava, selected based on the absence of macroscopic xenolithic material, were collected and analysed in two different laboratories (LMV Clermont-Ferrand and Centre de Recherches Pétrographiques et Géochimiques, Nancy) by using conventional ICP-AES techniques. Whole-rock major element compositions, CIPW norms, and A/CNK values of both samples are given in Table 1, as well as the analysis of a garnet-bearing metasedimentary enclave and selected published analyses of the Breziny andesite. The lava is a medium-K calc-alkaline acid andesite in the sense of Gill [1981] and is slightly metaluminous: A/CNK values lie between 0.96 and 0.98, except for the oldest analysis by Brousse et al. [1972]. The data suggest that nucleation of garnet, if actually grown from the bulk melt, is not related to an "excess Al" at the whole-rock scale.

4.2 Summary of andesite petrology

The lava is highly porphyritic—around 50 % phenocrysts (1–10 mm in size)—reflecting extensive crystallisation at depth prior to eruption. In thin-section, in addition to plagioclase, a few types of hornblende phenocrysts are observed, notably green- and brown-coloured varieties (Figure 2A). Garnet occurs primarily as discrete crystals up to 15 mm in size and homogeneously distributed in the lava. All garnet megacrysts, except the perfectly euhedral one shown in Figure 2B, exhibit reaction rims mainly composed of plagioclase (Figure 2C) indicating non-equilibrium conditions within their host magma. It should be noted that beside these megacrysts, smaller, more or less corroded garnet grains also occur, in close association with brown hornblende (Figure 2D). Although no point counting was done in the field, garnet megacrysts are estimated to represent 1 % volume at most.

Inclusions of igneous texture, comprising rounded microgranular enclaves and coarser-grained hornblende-rich aggregates, are abundant. These are dominated by hornblende and plagioclase, with possible accessory biotite and orthopyroxene, but garnet was never found in these enclaves. For this reason, these inclusions are not considered further in this study. They are argued to represent early magmatic crystallisation products and crystal aggregates from their host or related magmas at depth. Apart from these igneous-looking inclusions, the most common enclaves are angular fragments of the country rocks.

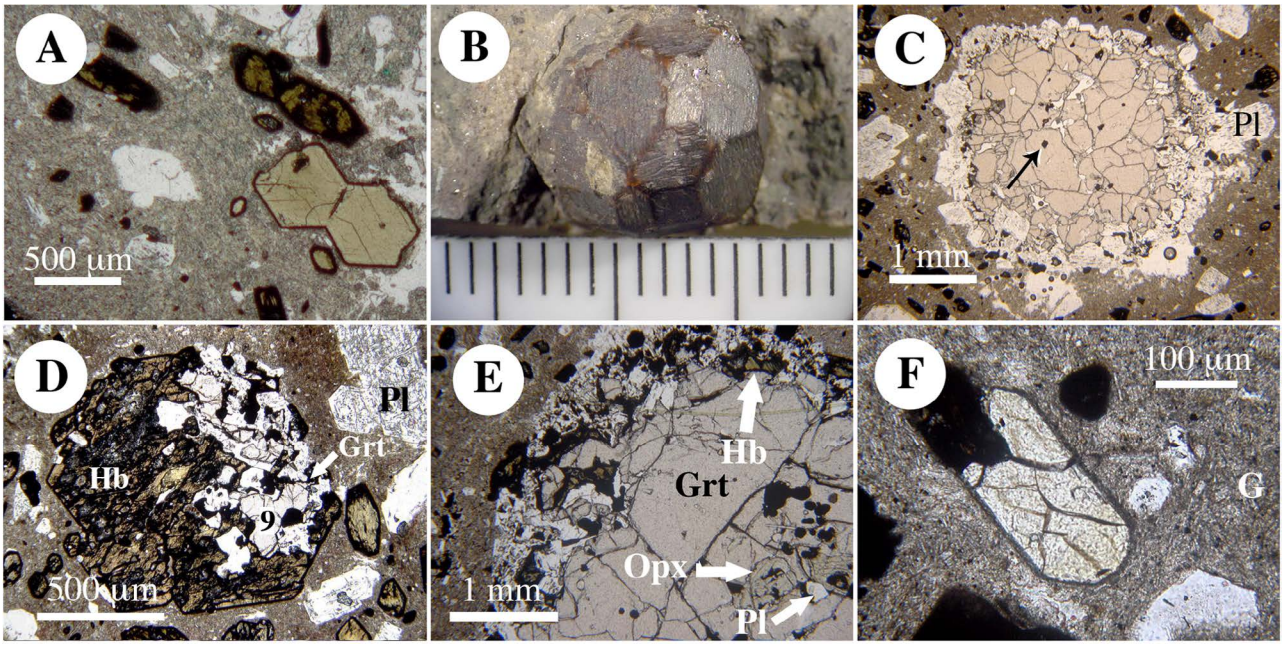

Figure 2: Main mineralogical characteristics of the Breziny garnet-bearing andesite (SK8). Mineral abbreviations after Whitney and Evans [2010]. [A] Microphotograph showing the juxtaposition of two different types of amphibole exhibiting various degrees of decomposition into opaque pseudomorphs and hence recording contrasting histories. The green one (lower right corner) is almost devoid of any decompression reaction rim and just exhibits oxidation effect (black rim). Brown crystals, on the contrary, are partly or almost completely oxidised to opacite. Plane-polarised light (PPL). [B] Macrophotograph of a perfectly euhedral garnet megacryst. Scale bar is millimetric. [C] Representative example of garnet megacryst with its reaction corona almost exclusively composed of plagioclase. Arrow inside garnet marks ilmenite inclusion (black). PPL. [D] Microphotograph of a euhedral phenocryst of brown hornblende with relict garnet inside. Black number in the garnet refers to analysis in Table 6. PPL. [E] Orthopyroxene inclusions in the core of a garnet megacryst whose reaction corona is characterised by brown hornblende. PPL. [F] Rounded microphenocryst of orthopyroxene. G = groundmass. PPL.

They correspond either to fragments of the Tertiary sediments or to metamorphic rocks from the crystalline basement. Their angular shape suggests that these metamorphic fragments were derived from the walls of the magma conduit at moderate depths, and no special attention has been paid to these inclusions. By contrast, two rare types of garnet-bearing enclaves were found that will be described in some detail. The first one corresponds to gneissic xenoliths, the second to garnetite nodules. Since the objective of this paper is to assess the origin of garnet in andesite, these two types indeed bear a critical interest. Finally, it is noteworthy that no clear evidence for magma mixing was observed at the sample scale, except a faint infra-millimetric layering that occurs sporadically.

A major feature of the Breziny andesite is its microscale heterogeneity, manifested in particular by the juxtaposition of several types of hornblende phenocrysts. This suggests that components of the andesite have been mixed together from different magma batches; however, the main point of interest is that mineral inclusions in garnet megacrysts do not match closely the phenocryst population of the host rock. If the green hornblende variety is common as a phenocryst, it was never found in association with garnet, contrary to the brown variety that most frequently corrodes and includes garnet. On the other hand, along with ubiquitous plagioclase inclusions, orthopyroxene inclusions are common in garnet (Figure 2E). As orthopyroxene is almost absent as a phenocryst in the groundmass (only three microphenocrysts were found in more than forty thin-sections: Figure 2F) it appears that garnet megacrysts are antecrysts grown—together with plagioclase and orthopyroxene—from a magma significantly different from the present-day bulk lava. In the absence of contrary evidence, it is assumed that this primary association Grt-Pl-Opx is in equilibrium with respect to the temperature and the pressure at which these minerals equilibrated. As this early-crystallised assemblage is composed of anhydrous minerals, this suggests that crystallisation of garnet megacrysts occurred at relatively higher-T and/or under more strongly H_2O-undersaturated conditions than those necessary for hornblende formation [Green 1972; Alonso-Perez et al. 2009]. Two explanations may account for this situation: 1) a primitive "dry" garnet-bearing magma was subsequently modified as a result of a water influx, leading to orthopyroxene destabili-

Table 1: Whole-rock composition of the andesite of Breziny (analyses 1–5) and a garnet-bearing metasedimentary enclave (analysis 6). Analyses 1, 2, and 6: this study; 3: Analysis S-B1 from Harangi et al. [2001]; 4: Analysis "Breziny" from Irving and Frey [1978]; 5: Analysis 11 from Brousse et al. [1972]. Below: A/CNK (aluminium saturation index) = molar $Al_2O_3/(K_2O+Na_2O+CaO)$ and CIPW norm of the andesite. n.d. = not detected.

	1	2	3	4	5	6
SiO_2	60.30	59.37	60.84	60.79	57.82	41.07
TiO_2	0.73	0.70	0.71	0.68	0.90	1.47
Al_2O_3	17.10	17.36	17.38	17.22	17.82	26.90
Fe_2O_3	6.64	6.66	6.72		5.83	15.18
FeO				5.75	2.15	
MnO	0.14	0.13	0.14	0.13	n.d.	0.13
MgO	2.35	2.30	2.34	2.24	1.92	3.70
CaO	5.82	5.85	5.90	5.84	7.61	4.16
Na_2O	3.02	3.01	3.13	3.06	2.26	2.04
K_2O	1.89	2.01	2.11	2.09	1.68	3.30
P_2O_5	n.d.	0.20	0.22	0.20	0.04	0.16
LOI	2.34	2.26	0.38	1.88	2.20	1.86
Total	100.33	99.85	99.87	99.88	98.03	99.97
A/CNK	0.97	0.98	0.96	0.96	0.92	
Qz	17.58	16.48	16.94	17.68	17.31	
Crn	0.00	0.08	0.00	0.00	0.00	
Or	11.17	11.88	12.47	12.35	9.93	
Ab	25.55	25.47	26.49	25.89	19.12	
An	27.52	27.72	27.14	27.08	33.52	
Di	1.11	0.00	0.57	0.49	3.31	
Hy	10.21	10.75	10.51	10.05	9.13	
Mt	2.99	2.97	3.06	2.90	3.56	
Ilm	1.39	1.33	1.35	1.29	1.71	
Ap	0.00	0.47	0.52	0.47	0.09	
Total	97.53	97.14	99.04	98.21	97.69	
Di/Hy	0.11	0.00	0.05	0.05	0.36	

sation in the groundmass and massive crystallisation of amphibole; 2) the present-day hornblende-bearing magma results from the blending of two (or more) magma batches, one of them carrying garnet. As shown by the coexistence of several distinct types of amphibole, evidence for magma mingling is clear. On the other hand, orthopyroxene remnants in hornblende phenocrysts are uncommon and for this reason the first hypothesis is not favoured.

4.3 Petrology of the garnet-bearing enclaves

Garnet-bearing enclaves comprise high-grade gneissic xenoliths and garnetite lenses solely composed of aggregated garnet grains. Evaluating their genetic relationship to the host magma is likely an important factor in inferring the petrogenesis the andesite.

4.3.1 *High-grade gneissic xenoliths*

Two xenolith samples, a few cm in size, have been examined. They appear as poorly-foliated dark gneissic fragments, rimmed by a light-coloured corona mainly composed of interlocking crystals of plagioclase (Figure 3A). The chemical analysis of one of these enclaves is given in Table 1 (analysis 6). It is characterised by a very low SiO_2 content (41.1 wt%) and a very high Al_2O_3 content (26.9 wt%). This melt-depleted, bulk-rock composition suggests that this xenolith represents restite or readjusted restite material and may therefore be genetically linked to the genesis of garnet megacrysts.

The core of the xenoliths is a fine- to medium-grained gneiss consisting primarily of plagioclase and biotite, associated with millimetric garnets (Figure 3B) and abundant fibrolitic sillimanite. Spinel is a minor constituent, commonly accompanied by corundum. Accessory ilmenite, apatite, and zircon complete the mineral assemblage along with subhedral crystals of monazite (Figure 3C). Biotite flakes and fibrolite folia define a weak foliation (Figure 3A and D), statically overgrown by coarse-grained plagioclase. Biotite generally exhibits embayed rims and contains oxidised spinel grains that outline its instability. Quartz and K-feldspar are typically absent, and any evidence of melt is missing: no film of glass, either fresh or devitrified, was found along the grain boundaries and melt inclusions are conspicuously absent.

The width of the reaction-rims varies from a thin overgrowth to an accumulation of interlocked plagioclase associated with a brown hornblende (Figure 3D). Plagioclase develops euhedral faces against the groundmass and the size, habit, and nature of both minerals demonstrate that the corona is magmatic. It is composed of minerals that already saturated the enclosing melt, and it is likely that the gneissic core primarily acted as a support for the growth of magmatic crystals. Minor garnet and orthopyroxene complete the mineralogy of the reaction rim. As orthopyroxene is unknown in these enclaves, magmatic origin of this phase is beyond doubt, even though the whole corona assemblage (plagioclase-brown hornblende-Ca-rich garnet-orthopyroxene) does not necessarily constitute an equilibrium paragenesis. Finally, biotite inclusions are frequent in the brown hornblende of the corona suggesting that amphibole crystallised in response to a melting event affecting a biotite-bearing protolith.

In situ U-Th-Pb dating of monazite [Didier et al. 2015] allows the precise origin and significance of these gneissic enclaves to be determined. Three generations of monazites, correlated with the breakdown and/or growth of plagioclase and garnet, were indeed described in one of these samples [Didier et al. 2015]. The youngest event, dated at 13.4 ± 0.2 Ma, is consistent with the age of 13.3 ± 0.2 Ma determined on zircons shielded within garnets from the same andesite [Bouloton and Paquette 2014]. This age represents

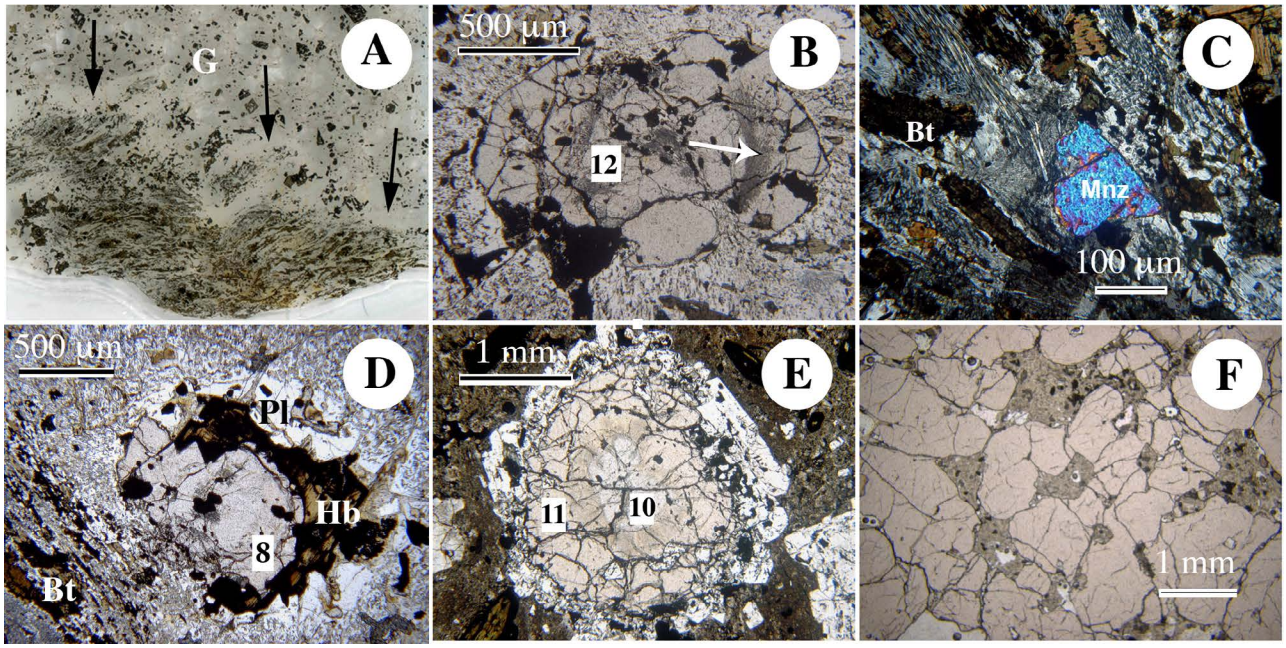

Figure 3: Petrographic features of the metasedimentary enclaves and garnetite lenses. Mineral abbreviations after Whitney and Evans [2010]. Numbers in white boxes refer to garnet analyses in Table 2. [A] General appearance of a metasedimentary enclave (thin-section scan, width of view 40 mm). The well-developed cleavage is marked by biotite. The coarse-grained reaction-rim appears as a light-coloured, leucocratic halo (arrows). Enclosing lava is visible in the upper part (G = groundmass). [B] Microphotograph of a typical metamorphic garnet in the core of a metapelitic enclave. Ilmenite inclusions (black) are numerous, and aggregates of fibrous sillimanite (white arrow) outline an internal irregular ring. Also present are plagioclase and biotite in the matrix around garnet. PPL. [C] Monazite crystal. Crossed-polarised light. [D] Close-up view of the granular selvage developed around metapelitic inclusions. Garnet and brown hornblende in a matrix of plagioclase (clear or altered). Note the slight difference in colour between the core of the garnet and its rim (pinkish). Number in the white box refers to garnet analysis in Table 6. Biotite (Bt) in the lower left corner marks the edge of the gneissic xenolith. PPL. [E] Composite garnet megacryst most probably expelled from the neighbouring (5 mm) metasedimentary enclave. The colourless core of metamorphic origin and the large magmatic overgrowth, slightly coloured in light-orange, are clearly distinct. The large reaction-rim is mainly composed of plagioclase (white). See X-Ray map and corresponding line profile of this garnet in Figure 9. PPL. [F] Garnetite enclave, characterised by the aggregation of small (mm-sized) individual garnet crystals. Voids between garnet grains are filled with plagioclase, a few oxides and secondary phases, mainly carbonates and a mineral of the zeolite group. PPL. Corresponding X-Ray map is given in Figure 5F. Numbers in the white boxes refer to garnet analyses in Table 6.

the time of the enclavement, whereas the oldest age at 309 ± 9 Ma is assumed to date the melting episode. The third group of ages ranges from 43 to 70 Ma and is ascribed to mixing ages [Didier et al. 2015]. Partial melting thus occurred long before incorporation of the gneiss in the lava, explaining the lack of any trace of melt in the enclave. These silica-deficient xenoliths are genetically related to a much older crustal-scale melting event of Variscan age, and though scavenged from the deep crust (pressure estimates up to 1.1 GPa have been proposed by Didier et al. [2015] for the magmatic reaction corona) they are not restites for their andesitic host. These metasedimentary enclaves represent a refractory material, only superficially affected by the Miocene magmatic event.

4.3.2 *Garnetite lenses*

Garnetite lenses are very scarce and correspond to coherent aggregations of garnet, approximately 3–5 cm in length, rimmed by a thin plagioclase corona. These lenses are almost exclusively composed of mm-sized garnet crystals tightly aggregated to each other. Minor interstices between the garnets are mainly filled with "plumose" feldspar, together with oxides and secondary phases (Figure 3F). A few small inclusions of orthopyroxene, apatite, and zircon occur in garnet, but oxide inclusions are lacking.

5 Detailed mineralogy of the phases coexisting with garnet

Major (amphibole-plagioclase-orthopyroxene) and minor phases (biotite-FeTi oxides-apatite-zircon) coexisting with garnet are described in this section (Section 5); garnet is the subject of a specific section (Section 6).

5.1 Major mineral phases

5.1.1 *Amphibole*

Hornblende is the most abundant mafic mineral in the rock. It ranges between 1 and 10 mm in length and varies from pristine euhedral to slightly rounded crystals. According to their general optical appearance, several distinct types may be identified in thin-section: 1) a light green pleochroic variety (Figure 4A), generally inclusion poor (rare apatite and plagioclase), and commonly associated with plagioclase in glomeroporphyritic clots; 2) a brown variety that mainly occurs in the reaction coronas around the garnet-bearing metasedimentary enclaves but is also found as discrete phenocrysts (Figure 4B); 3) a "brown-black" variety, rich in inclusions of plagioclase, apatite, orthopyroxene, and Fe-Ti oxides, and that is partly or completely pseudomorphed by opacite (Figure 4C); 4) a composite variety, such as that shown in Figure 4G, characterised by a marked contrast between a light yellow-brown core and a darker brown rim. Green hornblende phenocrysts are never in contact with garnet, contrary to the brown hornblende that commonly occurs in the reaction-rims around garnet megacrysts (Figure 2E). Moreover, garnet inclusions in brown hornblende phenocrysts are common (Figure 2D) and the later constitutes, together with garnet and plagioclase, peculiar aggregates (Figure 4J) that could, in part, represent disseminated fragments of the reaction coronas surrounding the metasedimentary enclaves. The common presence of biotite inclusions (Figure 4B) is a major characteristic of these brown amphiboles.

Almost all amphiboles show reaction textures with the enclosing magma, the breakdown products varying largely in size. Fine- to medium-grained intergrowths of clino- and orthopyroxene, plagioclase, and oxides identified around some amphiboles are interpreted to reflect a decrease in water fugacity of the melt during magma ascent [Murphy et al. 2000]. These decompression-related breakdown textures differ significantly for brown and green hornblendes (Figure 2A). Brown hornblendes have larger reaction coronas than the green ones, suggestive of a longer time of reaction with the ambient melt [Rutherford and Hill 1993], possibly due to a lower rate of ascent, or a long-lasting shallow magma storage. On the other hand, opacite, the black product that develops around crystals and along cleavages and cracks, should be due to oxidation and could be formed during the latest oxidation stage in the extrusion dome [Murphy et al. 2000].

Compositions of representative hornblende types are given in Table 2. All amphiboles belong to the calcic group and correspond to tschermakites or magnesiohastingsites in the IMA terminology [Leake et al. 1997]. Variations in Al_2O_3 among the whole amphibole series are low (from 10.5 to 14.5 wt%) as are the variations of this parameter from core to rim in zoned crystals. Differences in TiO_2 content are larger (1.3 to 2.4 wt%), as well as variations in Mg# number (Mg# = $Mg_2^+/Mg_2^+ + Fe_2^+ \times 100$), which ranges from 70 for green hornblendes to less than 50 for brown ones. This higher Mg# number may either indicate that the green variety equilibrated at a higher temperature [Day et al. 1992] or at a higher oxygen fugacity [Moore and Carmichael 1998]; however, amphiboles with a higher Mg# might also have simply crystallised from a parental magma richer in MgO [Green 1992].

5.1.2 *Plagioclase*

Plagioclase size ranges from small microlites (10 µm) to large euhedral phenocrysts up to 7–8 mm, and frequently occurs as inclusions in mafic minerals. For instance, it commonly defines concentric internal rings in garnet. Plagioclase inclusions are also common in brown hornblendes (An 55–80) but much rarer in green ones, though both minerals are commonly interlocked in milli to centimetric glomerocrysts. Core to rim variations in anorthite content are noteworthy, from An 70–80 to An 44. Tiny rounded plagioclase inclusions, looking like residual minerals, also occur in garnet.

Representative analyses of the different types of plagioclase are given in Table 3. Except the microlites that are significantly less calcic (An 40–45), all other types have broadly similar compositions and range from An 55 to An 85. More calcic compositions (An > 85) have only been observed in reaction-rims around the most strongly resorbed garnet megacrysts. Both phenocrysts and inclusions generally show compositional zoning. In most cases, they exhibit normal and slight oscillatory zoning; sieve-textured and resorbed crystals as well as reverse zoning are rather uncommon. In the absence of a detailed study of their zoning patterns, distinguishing different populations of crystals among the whole set of plagioclase was not attempted. Incidentally, orthoclase content never exceeds 3 %, whatever the type of plagioclase; the only exception concerns crystals intergrown with clinopyroxene in the breakdown products of brown hornblende, which can reach 7.5 % Or.

5.1.3 *Orthopyroxene*

Orthopyroxene occurs mostly as inclusions in garnet megacrysts, either as shielded grains (Figure 2E) or as microphenocrysts, up to 400 µm, present in large crystallised melt pools. Orthopyroxene also consti-

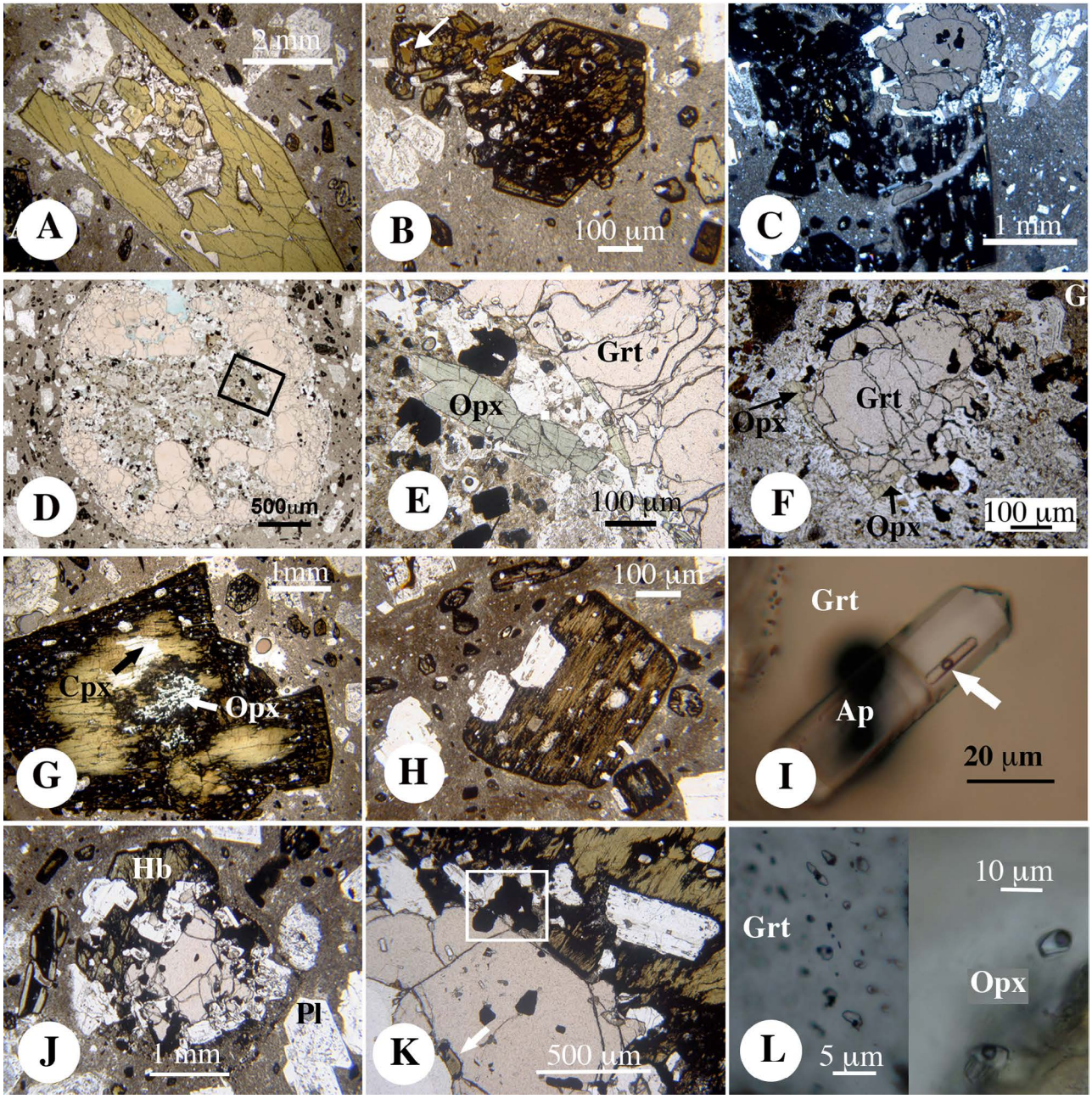

Figure 4: Transmitted light photomicrographs of the main phases. Mineral abbreviations after Whitney and Evans [2010]. [A] Perfectly euhedral green hornblende phenocryst almost devoid of any reaction-rim. [B] Brown hornblende phenocryst with biotite inclusions (arrows). [C] Photomicrograph (partly crossed polariser) of a "brown-black" hornblende phenocryst almost totally transformed in opacite. Partly enclosed garnet crystal shows a plagioclase corona, attesting that it was in contact with the melt and developed a reaction-rim before being enclosed by amphibole. [D] General view of the atoll-like garnet megacryst described in the text. Black box corresponds to the enlarged view in Figure 4E. Thin-section scan, width of view 20 mm. [E] Boxed area in Figure 4D. Orthopyroxene crystal in the central cavity of the atoll-like garnet. [F] Garnet-orthopyroxene association in the reaction-rim of a metasedimentary inclusion. The Ca-poor colourless core of the garnet is clearly visible. Groundmass is visible at upper right of the photograph. [G] Complex amphibole, with corroded remnants of ortho- and clinopyroxene in the core. [H] Rounded, partly resorbed biotite phenocryst. [I] Euhedral crystal of apatite included in garnet, showing a negative crystal-shaped melt inclusion with its typical shrinkage bubble (arrow). The black spot in the centre of the photograph corresponds to an ilmenite inclusion situated at a higher level. [J] Crystal clot of brown hornblende, garnet and plagioclase. The residual aspect of garnet is clearly visible. [K] Only known example of inclusion of brown hornblende in garnet (white arrow), indicating that both minerals could in some cases actually co-crystallise. White box corresponds to the Ti-oxides aggregate shown in Figure 5C. [L] Examples of the scarce and tiny melt inclusions respectively found in garnet (left) and orthopyroxene (right).

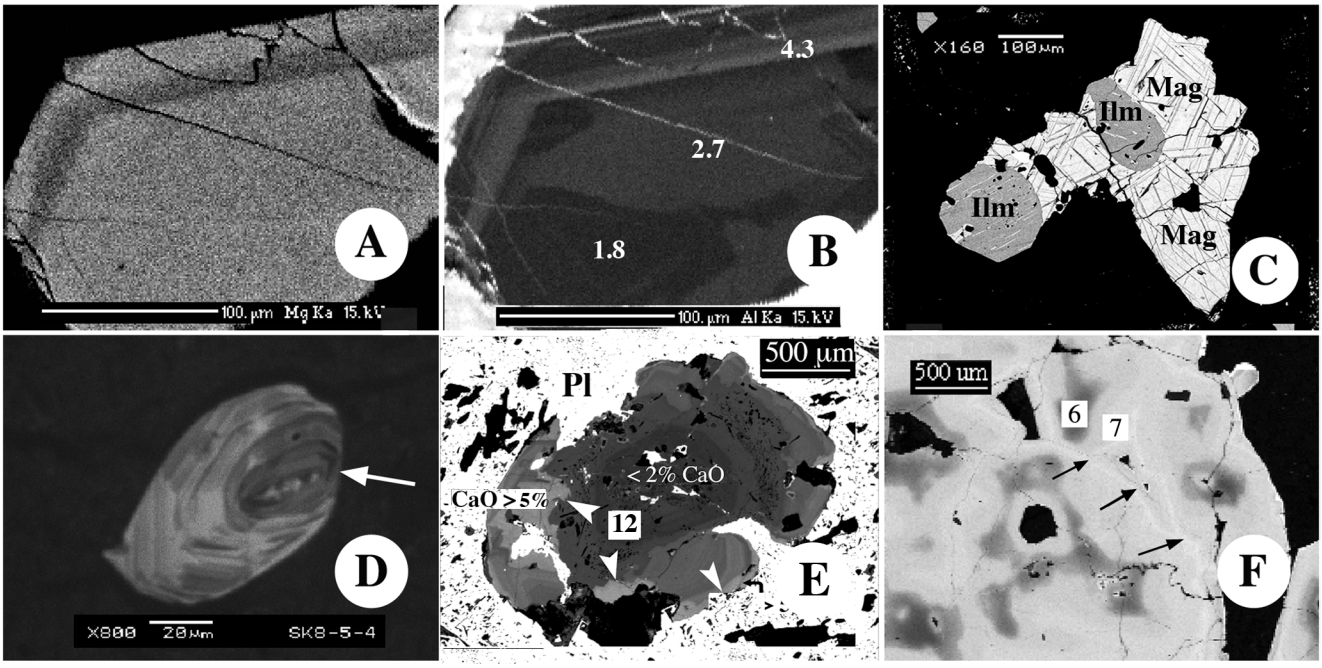

Figure 5: Some details about mineralogy. Mineral abbreviations after Whitney and Evans [2010]. [A] Mg X-Ray SEM image showing euhedral concentric zoning pattern in orthopyroxene. Light grey represents higher, dark grey lower concentration in Mg. [B] In addition to concentric zonation, sector zoning is evidenced by the Al X-Ray image in the core of the orthopyroxene. Numbers correspond to Al_2O_3 content in wt%. [C] BSE image of coexisting iron-titanium oxides. Both minerals exhibit exsolution lamellae expressing intra-oxide reequilibration during cooling (oxidation-exsolution of ilmenite lamellae from titano-magnetite and reduction-exsolution lamellae of magnetite from ilmenite). [D] Cathodoluminescence image of a free zircon in the groundmass showing local magmatic corrosion and rounding of the crystal faces (arrow). [E] EPMA Ca X-Ray map of the metamorphic garnet crystal shown in Figure 3B. A dark grey Ca-poor internal core (CaO < 2 wt%) is clearly visible; it is truncated (white arrows) by the outer magmatic overgrowth (light grey) much richer in Ca (CaO > 5wt%). Number in the white box refers to garnet analysis in Table 6. [F] EPMA Mn X-Ray map of a garnetite inclusion; each garnet crystal is characterised by a Mn-poor core (dark grey), while grain boundaries (arrows) are outlined by much Mn-richer narrow rims (white). Numbered spots in white squares refer to garnet analyses in Table 6.

tutes a coarse-grained association with plagioclase in the central cavity of a spectacular atoll-like garnet (Figure 4D and Figure 4E), while some inclusions occur in garnet from the garnetites. Minor orthopyroxene is also present in the magmatic selvage developed around metasedimentary enclaves (Figure 4F) and in some reaction rims around garnet megacrysts. By contrast, very few microphenocrysts (Figure 2F) were identified in the groundmass. Otherwise, orthopyroxene occurs as inclusions in brown hornblende, and it was exceptionally found, together with clinopyroxene remnants, as relics shielded in a complex hornblende phenocryst (Figure 4G).

Compositions of representative crystals are given in Table 4. The whole compositional range of inclusions in garnet—either megacrysts or garnetites—is restricted to Fe-rich compositions (Mg# = 44–47). These values are much lower than those expected (about Mg# > 60) for phenocrysts grown from an average andesitic melt. Compared to inclusions in garnet, orthopyroxene microphenocrysts and those occurring in reaction-rims—either around metasedimentary enclaves or garnet megacrysts—have a slightly higher Mg# (51–52). Not surprisingly, the highest value (Mg# = 0.56) is shown by the relictual orthopyroxene included in hornblende. Finally, the most important point concerns the high variability of orthopyroxene in Al content. Due in particular to sector zoning (Figure 5B), Al_2O_3 indeed may vary from 1.8 to 4.3 wt% in the same crystal. It is worth noting that sector zoning appears to be the normal mode of crystallisation, rather than the exception, for rapidly grown crystals [Schwandt and McKay 2006].

5.2 Minor mineral phases

5.2.1 *Biotite*

Only four phenocrysts (Figure 4H) have been found in more than forty thin-sections. This extreme scarcity suggests that these are "exotic" crystals that may have grown in another magma batch and were later introduced in their present-day host. By contrast, abundant biotite inclusions are preserved in brown horn-

Table 2: Representative major element analyses of amphibole. Cations based on 23 oxygens (apfu). Structural formulae calculated with the `ProbeAmph` spreadsheet [Tindle and Webb 1994]. Comments on occurrence: 1–2: green hornblende phenocrysts; 3: green hornblende from a Hb-Pl clot; 4–5: complex hornblende shown in Figure 4G; 6–7: brown hornblende phenocryst; 8: brown hornblende associated with garnet; 9: brown hornblende in reaction rim of a metasedimentary enclave; 10: brown hornblende with Opx inclusion; 11–12: "brown-black" opacitised hornblende phenocrysts. Mg# = 100Mg/(Mg+Fet) in moles, where Fet is total iron.

	1	2	3	4	5	6	7	8	9	10	11	12
				core	rim	core	rim					
SiO_2	41.38	40.07	41.71	42.70	41.51	42.18	41.61	40.87	43.40	41.01	41.2	41.47
TiO_2	2.19	2.44	2.40	2.01	1.38	1.57	1.54	1.32	1.29	1.39	1.27	2.04
Al_2O_3	13.58	14.46	13.43	12.47	12.58	12.57	12.37	14.23	10.53	12.64	12.24	12.35
FeO	11.63	15.60	11.23	12.49	20.69	20.35	19.16	18.09	19.73	20.62	20.87	21.54
MnO	0.14	0.20	0.15	0.10	0.40	0.46	0.44	0.54	0.51	0.48	0.48	0.48
MgO	14.16	10.3	14.76	13.12	8.73	9.57	10.13	10.39	10.88	9.44	9.13	8.83
CaO	11.04	11.21	11.16	11.77	10.01	9.35	9.95	9.09	8.74	9.47	9.29	9.45
Na_2O	2.31	2.01	2.21	1.88	1.70	1.94	1.96	2.05	1.76	2.16	2.53	1.80
K_2O	0.77	0.84	0.81	0.75	0.81	0.52	0.53	0.55	0.42	0.66	0.53	0.66
Total	97.20	97.13	97.86	97.29	97.81	98.51	97.69	97.13	97.26	97.87	97.54	98.62
Cations based on 23 oxygens												
Si	5.98	5.95	5.97	6.24	6.13	6.10	6.09	5.92	6.27	6.01	6.08	6.05
Al iv	2.02	2.05	2.03	1.76	1.87	1.90	1.91	2.08	1.73	1.99	1.92	1.95
Al vi	0.29	0.48	0.23	0.38	0.32	0.25	0.22	0.35	0.07	0.20	0.21	0.17
Ti	0.24	0.27	0.26	0.22	0.15	0.17	0.17	0.14	0.14	0.15	0.14	0.22
Fe_3^+	1.05	0.71	1.10	0.58	1.44	1.77	1.58	1.93	2.10	1.77	1.66	1.75
Fe_2^+	0.36	1.22	0.24	0.95	1.12	0.69	0.77	0.26	0.28	0.76	0.91	0.87
Mn	0.02	0.03	0.02	0.01	0.05	0.06	0.05	0.07	0.06	0.06	0.06	0.06
Mg	3.05	2.28	3.15	2.86	1.92	2.06	2.21	2.25	2.35	2.06	2.01	1.92
Ca	1.71	1.78	1.71	1.84	1.58	1.45	1.56	1.41	1.35	1.49	1.47	1.48
Na	0.65	0.58	0.61	0.53	0.49	0.54	0.56	0.58	0.49	0.61	0.72	0.51
K	0.14	0.16	0.15	0.14	0.15	0.10	0.10	0.10	0.08	0.12	0.10	0.12
Total	17.5	17.52	17.47	17.52	17.22	17.09	17.22	17.09	16.92	17.23	17.29	17.11
Mg#	68.5	54.1	70.1	65.2	42.9	45.6	48.5	50.6	49.6	44.9	43.8	42.2

blende phenocrysts (Figure 4B), as well as in hornblende intergrown with plagioclase in the granular selvages surrounding metapelitic inclusions. These biotite inclusions testify that crystallisation of the brown hornblende occurred during a melting process involving a biotite-bearing protolith. Finally, a few rounded biotite inclusions also occur in garnet; like the previous ones, these shielded crystals may correspond to remnants from a biotite reactant involved in a garnet-producing melting reaction.

Compositions of the different types of biotite are given in Table 5. Restitic biotites in the metasedimentary xenoliths and inclusions in garnet have similar Mg numbers (mean Mg# = 0.54) and show the highest Ti contents, up to 0.53 and 0.51 per formula unit (pfu), respectively. Biotite phenocrysts and inclusions in brown hornblende have broadly similar Ti contents (about 0.45 pfu), but differ significantly by their Mg number (mean Mg# = 0.47 and 0.57, respectively).

5.2.2 *Fe-Ti oxides*

Ilmenite and Ti-magnetite occur together in the groundmass and in the garnet-plagioclase-brown hornblende aggregates. Each of these oxides may exhibit exsolution lamellae of the other phase (Figure 5C), indicative of intra-oxide re-equilibration during cooling. By contrast, ilmenite is by far the most common iron-titanium oxide shielded in garnet megacrysts. It displays the lowest Mg/Mg+Fe ratio of all the ferromagnesian phenocrysts, most Mg# values being between 5 and 10. This suggests oxygen fugacities below the QFM buffer, a feature considered typical of peraluminous silicic magmas [Clemens and Wall 1981]. Magnetite occurs mostly among the breakdown products of hornblende. However, it is also known to coexist with orthopyroxene in the large melt pools trapped in garnet previously mentioned. Compositions of the different types of oxides are given in Table 5. Most of the

Table 3: Representative major element analyses of plagioclase. n.d. = not detected (below detection limit). Cations based on 32 oxygens (apfu). Comments on occurrence: 1–2: phenocrysts (max and min An%); 3: in association with green hornblende (Hb-Pl clot); 4: microlite; 5: in a metasedimentary xenolith; 6: in the crystalline corona around a metasedimentary xenolith; 7: inclusion in garnet; 8: in the core of the atoll garnet shown in Figure 4D; 9: in the granoblastic core of the composite garnet shown in Figure 6D; 10: in garnet reaction rim.

	1	2	3	4	5	6	7	8	9	10
SiO_2	49.27	56.83	48.64	57.16	57.32	51.78	51.53	52.23	49.74	52.91
TiO_2	n.d.	0.02	n.d.	n.d.	n.d.	0.03	0.04	n.d.	0.01	0.01
Al_2O_3	31.86	27.60	32.04	26.29	26.83	29.22	30.44	29.79	32.43	29.08
FeOt	0.17	n.d.	0.31	0.83	0.11	0.47	0.47	0.31	0.39	0.21
MnO	0.03	0.12	0.03	0.00	0.01	0.00	0.04	0.01	0.04	0.04
MgO	n.d.	n.d.	0.01	0.15	0.02	0.02	0.00	0.04	n.d.	n.d.
CaO	15.18	9.65	15.50	9.07	8.79	12.87	13.66	12.65	15.27	12.01
Na_2O	2.98	5.97	2.61	6.02	6.91	4.13	3.70	4.18	2.72	4.61
K_2O	0.11	0.29	0.07	0.50	0.39	0.19	0.08	0.13	0.07	0.18
Total	99.59	100.48	99.22	100.02	100.38	98.70	99.96	99.35	100.67	99.04
Cations based on 32 oxygens										
Si	9.05	10.17	8.98	10.30	10.27	9.54	9.39	9.54	9.03	9.68
Ti	0.00	0.00	0.00	0.00	0.00	0.00	0.01	0.00	0.00	0.00
Al	6.90	5.82	6.97	5.58	5.67	6.35	6.54	6.42	6.94	6.27
Fe	0.03	0.00	0.05	0.13	0.02	0.07	0.07	0.05	0.06	0.03
Mn	0.00	0.02	0.01	0.00	0.00	0.00	0.01	0	0.01	0.01
Mg	0.00	0.00	0.00	0.04	0.01	0.00	0.00	0.01	0.00	0.00
Ca	2.99	1.85	3.07	1.75	1.69	2.54	2.67	2.48	2.97	2.35
Na	1.06	2.07	0.94	2.10	2.40	1.48	1.31	1.48	0.96	1.64
K	0.03	0.07	0.02	0.12	0.09	0.05	0.02	0.03	0.02	0.04
Total	20.05	19.99	20.02	0.00	20.14	20.04	20.00	20.01	19.98	20.02
An	74.4	47.8	77.4	45.5	41.8	63.9	68.1	63.5	76.4	59.8
Ab	24.9	50.5	22.2	51.5	56	35	31.5	35.7	23.2	39.2
Or	0.6	1.7	0.4	3	2.2	1.1	0.5	0.8	0.4	1

analysed ilmenites contain less than 12 wt% Fe_2O_3, and there is no significant difference in Fe_2O_3 or MgO between ilmenite included in garnet and the discrete crystals occurring in the groundmass.

5.2.3 *Apatite and zircon*

Apatite occurs as cloudy microphenocrysts in the groundmass of all thin-sections and as inclusions in most phenocrysts of brown hornblende. Additionally, apatite inclusions in garnet are needle-like clear crystals whose magmatic origin is demonstrated by the presence of typical melt inclusions (Figure 4I). Zircon is commonly present as inclusions in the major phases, notably garnet, but is very scarce in the groundmass (Figure 5D). Crystals armoured in garnet range in size from a few microns up to 300 µm and are homogeneously distributed in garnet. *In situ* LA-ICP-MS U-Pb dating of the largest ones yielded Miocene ages [Bouloton and Paquette 2014], demonstrating the magmatic origin of their hosts. Moreover, it is worth noting that no zircon among the 17 grains investigated in SK8 had an obvious inherited nucleus.

5.2.4 *Missing phases of petrogenetic interest*

Interestingly, quartz does not occur as a phenocryst in the studied lava samples. However, this phase is not totally absent from the whole magma system: a few large-sized crystals occur in coarser-grained igneous enclaves, and a quartz phenocryst was observed in the large pool melt pool trapped in garnet—a former melt hollow, now crystallised—already mentioned and that will be discussed later (Section 6.3). Likewise, no clinopyroxene phenocryst has been found in the investigated samples. This phase was only observed as

4(2): 149 – 187. DOI: 10.30909/vol.04.02.149187

Table 4: Mean compositions of representative pyroxenes (analyses 1–10: Opx and 11: Cpx). n = number of analyses, s.d. = standard deviation (1Σ. Cations on the basis of 6 oxygens (apfu). Comments on occurrence : 1: microlites; 2: inclusions in garnetite; 3: microphenocrysts like the one shown in Figure 2F; 4: in crystalline corona around metasedimentary xenoliths; 5: microphenocrysts into the core of the atoll garnet shown in Figure 4D; 6: inclusions in garnet; 7: into the granoblastic core of the composite garnet shown in Figure 6D; 8: microphenocrysts in the crystallised melt hollows shielded in garnet (see Figure 10); 9: in reaction rims around garnet megacrysts; 10: Opx remnant in the complex hornblende shown in Figure 4G; 11: Cpx remnant in the same hornblende phenocryst.

	1		2		3		4		5		6		7		8		9		10		11	
	$n = 6$	s.d.	$n = 3$	s.d.	$n = 4$	s.d.	$n = 7$	s.d.	$n = 17$	s.d.	$n = 4$	s.d.	$n = 5$	s.d.	$n = 3$	s.d.	$n = 3$	s.d.	$n = 8$	s.d.	$n = 3$	s.d.
SiO_2	50.95	0.51	50.08	0.06	50.96	0.59	48.93	0.55	48.45	0.82	49.67	0.33	50.03	0.26	48.95	0.35	48.41	0.23	50.23	1.04	50.27	0.74
TiO_2	0.2	0.05	0.13	0.03	0.08	0.04	0.07	0.03	0.08	0.04	0.1	0.04	0.1	0.01	0.12	0.04	0.09	0.02	0.12	0.04	0.67	0.11
Al_2O_3	3.33	0.79	2.03	0.09	1.74	0.69	3.65	0.71	3.16	0.69	1.56	0.34	1.33	0.13	2.09	0.5	3.11	0.48	1.05	0.18	4.34	0.34
FeOt	29.37	1.59	31.89	0.08	28.00	0.61	29.37	0.79	29.42	0.69	31.94	0.42	32.85	0.46	32.54	0.3	29.29	0.18	28.86	1.71	7.81	1.72
MnO	1.01	0.07	0.78	0.02	0.99	0.09	1.31	0.21	1.92	0.22	0.86	0.05	1.08	0.06	0.8	0.25	1.32	0.15	0.94	0.03	0.24	0.04
MgO	14.88	0.95	15.38	0.04	18.3	0.44	16.44	0.48	15.65	0.58	14.65	0.27	14.36	0.16	14.11	0.21	15.83	0.11	17.17	1.39	13.81	1.11
CaO	0.79	0.13	0.57	0.01	0.61	0.02	0.48	0.17	0.69	0.07	0.62	0.02	0.66	0.03	0.45	0.02	0.64	0.02	0.84	0.09	21.78	0.52
Na_2O	0.19	0.07	0.01	0.01	0.01	0.01	0.02	0.01	0.02	0.02	0.02	0.01	0.02	0.03	0.04	0.03	0.02	0.02	0.02	0.02	0.39	0.05
K_2O	0.32	0.11	0.02	0.01	0.01	0.01	n.d.	0.01	n.d.	0.01	0.01	n.d.	0.01	0.01	n.d.	n.d.	n.d.	n.d.	0.01	0.01	0.03	0.03
Total	101.04		100.87		100.71		100.26		99.38		99.42		100.43		99.10		98.73		99.25		99.35	
Si	1.96		1.94		1.94		1.88		1.89		1.96		1.96		1.94		1.90		1.95		1.87	
Al iv	0.04		0.06		0.06		0.12		0.11		0.04		0.04		0.06		0.10		0.05		0.13	
Al vi	0.11		0.03		0.01		0.05		0.03		0.03		0.02		0.04		0.04		0.00		0.06	
Ti	0.01		0.00		0.00		0.00		0.00		0.00		0.00		0.00		0.00		0.00		0.02	
Fe_3^+	0.00		0.03		0.05		0.07		0.08		0.01		0.02		0.02		0.06		0.05		0.06	
Fe_2^+	0.94		1.00		0.84		0.88		0.88		1.04		1.06		1.06		0.90		0.89		0.19	
Mn	0.03		0.03		0.03		0.04		0.06		0.03		0.04		0.03		0.04		0.03		0.01	
Mg	0.85		0.89		1.04		0.94		0.91		0.86		0.84		0.83		0.92		0.99		0.77	
Ca	0.03		0.02		0.03		0.02		0.03		0.03		0.03		0.02		0.03		0.04		0.87	
Na	0.01		0.00		0.00		0.00		0.00		0.00		0.00		0.00		0.00		0		0.03	
Total	3.99		4		4		4		4		4		4		4		4		4		4	
Mg#	0.47		0.47		0.55		0.52		0.51		0.45		0.44		0.44		0.51		0.56		0.8	
Wo	1.7		1.2		1.3		1		1.5		1.3		1.4		1		1.4		1.8		46.1	
En	45.8		45.0		52.2		48.3		46.4		43.7		42.4		42.6		47.3		49.8		40.6	
Fe	52.5		53.7		46.5		50.7		52.1		55.0		56.2		56.5		51.4		48.5		13.3	

Table 5: Mean compositions of biotite and Fe-Ti oxides. *Total Fe as FeO. n = number of analyses; n.d. = not detected (below detection limit). Comments on biotite occurrence: 1: interpreted as biotite antecrysts; 2: inclusions in garnet; 3: inclusions in brown hornblende; 4: biotite in metasedimentary enclave. Comments on Fe-Ti oxides occurrence: 5: ilmenite inclusions in garnet; 6: ilmenite microcrysts in the groundmass; 7: ilmenite inclusions in brown hornblende. 8: titano-magnetite microphenocrysts in crystallised melt hollows shielded in garnet (see Figure 10). Recalculated values: FeO = 35.63, Fe_2O_3 = 52.27, Total = 99.55.

	Biotite				Ilmenite			Magnetite
	1	2	3	4	5	6	7	8
	$n = 4$	$n = 7$	$n = 2$	$n = 4$	$n = 14$	$n = 8$	$n = 4$	$n = 9$
SiO_2	35.23	35.74	35.83	34.78	0.01	0.01	0.03	0.13
TiO_2	3.85	4.19	3.84	4.04	48.48	49.28	46.87	5.19
Al_2O_3	15.77	15.66	15.42	16.91	0.20	0.08	0.48	5.32
FeO*	21.39	18.59	17.13	17.65	48.65	48.47	46.61	82.67
MnO	0.10	0.14	0.12	0.13	0.87	0.79	1.02	0.6
MgO	10.59	12.02	12.94	11.52	1.50	1.34	4.32	0.37
CaO	n.d.	0.02	0.08	0.04	0.09	0.05	0.05	0.01
Na_2O	0.54	0.36	0.14	0.49	0.02	0.01	0.01	0.02
K_2O	9.11	9.31	9.87	9.24	0.01	0.01	0.02	0.00
Total	96.58	96.04	95.36	94.80	99.83	100.05	99.4	94.31
Mg#	47.0	53.5	57.4	53.8				

remnants in a composite hornblende (Figure 4G) and in the fine-grained destabilisation products of amphibole. Composition of the residual clinopyroxene shielded in amphibole is given in Table 4, together with orthopyroxene analyses.

6 Attributes of the garnet: occurrence, composition and texture

Garnet mainly occurs as discrete megacrysts, 1 to 15 mm in size. It is dark red and an internal white ring of plagioclase inclusions commonly delineates the core of the megacrysts. This core greatly varies in size from one crystal to another. Almost all garnets exhibit white reaction coronas mainly composed of plagioclase (Figure 2C), often visible with the naked eye in hand samples. Only one example of unreacted, rim-free, perfectly euhedral garnet has been found (Figure 2B). Otherwise, the degree of resorption varies considerably and in some instances only a few relict examples of garnet remain at the centre of a spherical cluster of plagioclase crystals. Apart from plagioclase and minor phases (Fe-Ti oxides, apatite, and zircon) that are ubiquitous, orthopyroxene inclusions are quite common (Figure 2E). In contrast, inclusions of brown hornblende in garnet are exceedingly rare, though both minerals are commonly in contact: in fact, the tiny hornblende inclusion shown in Figure 4K is the only known example found in this work.

6.1 Garnet typology

On the basis of their mode of occurrence, garnets can be divided into four distinct types, described below in order of increasing abundance. Types 1 and 2 are rare and correspond respectively to metamorphic garnets from the high-grade metasedimentary xenoliths and aggregated garnets from the garnetite lenses. Type 3 garnet is slightly more abundant and corresponds to small, more or less corroded grains in close association with brown hornblende. Type 4 corresponds to the megacrysts disseminated in the lava and is by far the most common type, accounting for more than 80 % of the garnets examined.

6.1.1 *Type 1 garnet*

Type 1 garnet occurs as millimetric crystals (Figure 3B) in the gneissic core of the metasedimentary enclaves. X-ray imaging (Figure 5E) reveals the presence, around a Ca-poor core (CaO < 2 wt%), of a narrow rim (up to 200 µm wide) characterised by an abrupt increase in CaO (CaO > 5 wt%). This overgrowth shows an euhedral oscillatory zoning consistent with a magmatic origin. Conversely, the Ca-poor core is characterised by the presence of fibrolitic mats documenting its metamorphic origin.

6.1.2 *Type 2 garnet*

Type 2 garnet corresponds to the small garnet grains tightly aggregated to each other in the garnetites (Figure 3F). X-ray imaging (Figure 5F) reveals that each of the individual garnet grains is composed of a very

small Ca- and Mn-poor nucleus and a much larger overgrowth ring. Finally, a narrow rim (less than 20 µm) strongly enriched in Mn (Figure 5F) delineates the different garnet grains. Basically, the zoning pattern of Type 2 garnet is characterised, like the Type 1, by a sharp internal discontinuity providing evidence for a two-step history of garnet growth.

6.1.3 *Type 3 garnet*

Type 3 garnet corresponds to subordinate garnet grains associated with brown hornblende. It mainly occurs in reaction rims around metasedimentary enclaves (Figure 3D) and in discrete hornblende-plagioclase-garnet aggregates (Figure 4J) but is also present as inclusions in hornblende phenocrysts (Figure 2D). Whether these aggregates represent dispersed fragments of the reaction coronas is possible, but not demonstrated. Distinction is made hereafter between Type 3 garnets spatially and genetically related to the metasedimentary enclaves and the other two varieties.

Garnets associated with brown hornblende in the reaction rims of the metasedimentary enclaves display the same type of zoning as Type 1 garnets, but their CaO-rich rims are much larger, up to 700 µm. Again, these garnets clearly have both metamorphic and igneous growth histories. Garnets occurring in discrete brown hornblende-plagioclase aggregates and garnet included in brown hornblende phenocrysts are slightly different. The compositional gap between core and rim is less pronounced, possibly implying some kind of dissolution-reprecipitation process. These Type 3 garnets may either record a more advanced stage of transformation than those occurring in the reaction rims of the metasedimentary enclaves or, alternatively, express a different, purely magmatic history (see Section *9.2.1*).

Additionally, textural relations between garnet and brown amphibole are two-fold. Figure 4K suggests that both minerals could have co-crystallised, but garnet occurs in most cases as corroded relics in amphibole (Figure 2D and Figure 4J). This rather implies a reactional link between the two minerals, possibly in response to a variation of a_{H_2O} in the magma. Indeed, HT-HP experiments show that increasing a_{H_2O} may cause the destabilisation of garnet according to the reaction Garnet + Melt → Hornblende [Alonso-Perez et al. 2009].

6.1.4 *Type 4 garnet megacrysts*

Figure 6 is a compilation of X-ray images showing the common characteristics of the megacrysts and the differences from one crystal to the other. Plagioclase is by far the most common major phase included in garnet. Orthopyroxene inclusions (up to 0.8 mm in size) are abundant, in contrast with brown hornblende inclusions that are exceedingly rare. Rounded, tiny biotite and plagioclase inclusions are rare, and quartz or sillimanite inclusions are totally lacking. This absence puts strong limits to the possibility that garnet could be the peritectic product of a melting reaction involving a metapelitic protolith.

Together with needle-like apatite and zircon, ilmenite is a characteristic minor inclusion. Additionally, sulphides rarely are found. The origin of ilmenite grains, disseminated in their whole host, is currently unknown; they may correspond to magmatic or inherited residual minerals. Trails of fluid inclusions along healed fractures are common; typical melt inclusions on the other hand are rare (Figure 4L). Due to their small size (less than 5 µm), the composition of these glasses could not be correctly determined.

Among the whole set of studied garnets, two megacrysts are quite particular, in that their core is significantly different from their rim. These crystals are "composite" garnets, a term already used by Harangi et al. [2001] to describe such grains and willingly reused here for the sake of comparison. The first composite garnet is characterised by an inner core with a noritic assemblage (Opx+Pl+Grt), mantled by a magmatic garnet overgrowth (Figure 6C and 6D). The question arises of the nature of this core, that may either represent a rock fragment inherited from the source region or a piece issued from a cannibalised "proto-pluton" reactivated during injection of new magma. Whatever its exact nature, it is clear that this core acted as a mechanical support for the subsequent growth of the magmatic rim.

The second composite garnet is a strongly-zoned crystal (Figure 3E) that lies 5 mm apart from a metasedimentary enclave and is characterised by a Ca-poor core similar to Type 1 metamorphic garnets. This suggests that the Ca-poor core initially grew in the nearby enclave (or a similar one) and was later released into the silicate melt by disaggregation of the xenolith. Once released, it acted as a xenocryst out of equilibrium with its new environment and re-equilibrated with the host melt, by crystallising a Ca-richer overgrowth.

Finally, apart from these two composite garnets, a singular garnet megacryst must be mentioned, that looks like atoll-garnets sometimes found in retrogressed metamorphic rocks (Figure 4D). The central cavity of this garnet is occupied by a coarse-grained association of plagioclase (An 62–65) and orthopyroxene (Mg# = 51; Al_2O_3 up to 4 wt%), dispersed in a finely crystallised quartzo-feldspathic matrix whose texture is slightly different from that of the external groundmass. Whether the atoll-structure of the garnet is a primary feature due to special conditions of growth or the result of a later resorption episode is currently unknown. However, this garnet may indicate the coexistence, at some moment in the magma system history, of a magmatic garnet + orthopyroxene + plagioclase assemblage. In the absence of contrary evidence, it is assumed that plagioclase and orthopyroxene inclusions and their host garnet constitute an equilibrium assemblage.

6.2 Garnet chemistry

Compositions of some representative garnets are given in Table 6 and all analysed garnets are plotted in the ternary diagram (Fe + Mn)-Ca-Mg represented in Figure 7. Among the whole sample set, a few outliers clearly stand out. They correspond to the Ca-poor cores (CaO $\leqslant$ 2 wt%) of Types 1 and 2 garnets, specific of the metasedimentary enclaves and garnetite lenses (Figure 7A).

Type 4 garnet megacrysts form a coherent group with relatively little variation in composition within and between samples. Calculated andradite (Ca-Fe_3^+ end-member) ranges from 0.4 to $\leqslant$ 4 vol%, and schorlomite (Ca-Ti-end member) is < 1 vol%. For the sake of simplicity, garnet megacrysts can thus be considered in the quaternary system FeO-MgO-CaO-MnO. Total variations in CaO are quite weak, from 4.5 to 5.6 wt%. Variations in MgO are a little bit larger, from 3.3 to 5.9 wt%, and MnO content is less than 3.5 wt% with a mean value of 2.5 wt%. The total range of compositions of the garnet megacrysts may be expressed by the following formula in mol%: almandine 61–67 pyrope 15–25 grossular 10–15 spessartine 2–6 andradite 2–4. In terms of petrogenetically significant components, garnet megacrysts, on average, contain around 5 wt% CaO and 4.5 wt% MgO. It is worth noting that such compositions, in the metamorphic domain, characterise garnets from the more calcic rocks of the amphibolite and granulite facies [Popov 1983]. Otherwise, Type 2 garnets show the strongest compositional variations ever observed in SK8: garnet cores have the highest MgO content of all analyzed garnets (up to 8.6 wt%) and are the most strongly depleted in CaO (1.1 wt%). They are also characterised by their low MnO content (down to 0.7 wt%) compared to the mean content of the megacrysts (2.5 wt%). Such strongly Ca-depleted garnet cores are chemically reminiscent of peritectic garnets obtained in high-pressure melting experiments on metapelitic starting materials. By contrast, overgrowth rims of Types 1 and 2 garnets have a major element composition similar to that of Type 4 megacrysts, suggesting that they crystallised from a melt of broadly similar composition.

6.3 Zoning patterns

X-ray images of different garnet megacrysts are displayed in Figure 6, Figure 9A, and Figure 10. They show that the shape, pattern and number of garnet zones vary from crystal to crystal. Two extreme types of zoning occur: 1) broad zoning, consisting of nearly homogeneous wide rings, truncated by resorption surfaces (Figure 6A and 6D); 2) fine-scale, euhedral oscillatory zoning best shown by the Ti and Ca-elemental maps (Figure 6C and 6D). Resorption surfaces record discontinuities of crystal growth, reflecting more or less drastic changes in the magma environment during garnet crystallisation. Equatorial sections also show that plagioclase inclusions are often well-organised and define concentric rings parallel to the outer corona and alternating with almost inclusion-free zones (Figure 6A). Clearly, double rings of inclusions indicate that plagioclase and garnet co-crystallised from the same magma, even though some fluctuation in crystallisation-controlling parameters occurred.

Fine-scale oscillatory zoning (Figure 6D) may reasonably be the consequence of changes in intrinsic variables (temperature, pressure, or possibly water content in the melt). However, other features suggest the existence of more drastic changes. X-Ray imaging shows specifically that regular growth zoning is commonly interrupted by textural discontinuities along which the original zoning is resorbed and succeeded by the deposition of new, growth-zoned garnet (Figure 6D). These resorption episodes reflect intermediate periods of garnet undersaturation in the magma, whose origin could be *a priori* attributed to local kinetic phenomena or to large-scale mixing events. In this respect, strongly corrugated limits between rings (Figure 6D) are suggestive of a relatively high-degree of host-melt undersaturation and a faster rate of dissolution, far from the garnet-saturation surface. Therefore, it seems easier to interpret these dissolution features as evidence of mixing of magmas of contrasting composition and/or temperature, rather than consequences of simple changes in intensive parameters. However, EMPA traverses along equatorial sections (Figure 8, Figure 9B, and Figure 10E) show relatively mild variations and no clear and systematic correlation between elements is evidenced.

Additionally, X-Ray images reveal the occurrence of peculiar, quartzo-feldspathic, orthopyroxene-bearing inclusions up to 2 mm long (Figure 10). The skeletal shape of feldspars (Figure 10C and 10D) testifies that these inclusions represent former melt pools, apparently of rhyolitic composition (SiO_2 = 73 wt%; Table 7) as suggested by microprobe analyses using a defocussed beam (20 × 20 µm). The origin of these unusually large melt hollows, much bigger than common melt inclusions, is a challenging question. Melt inclusions of that size, trapped during the growth of their host have been reported in plagioclase and orthopyroxene phenocrysts of some crystal-poor calc-alkaline volcanics, where they are believed to reflect large undercooling caused by degassing [Crabtree and Lange 2011]. Such a mechanism is irrelevant to the present example, since a new garnet shell was subsequently formed. Owing to their size, it is beyond doubt that the various microphenocrysts observed in the hollows (orthopyroxene, Ti-magnetite, and quartz) were grown before melt trapping. Moreover, these hollows define a discontinuous ring that is slightly discordant on the euhedral zoning of garnet (Figure 10A) and thus clearly outline a discontinuity in garnet growth. The question arises of the significance of this discontinuity and the pre-

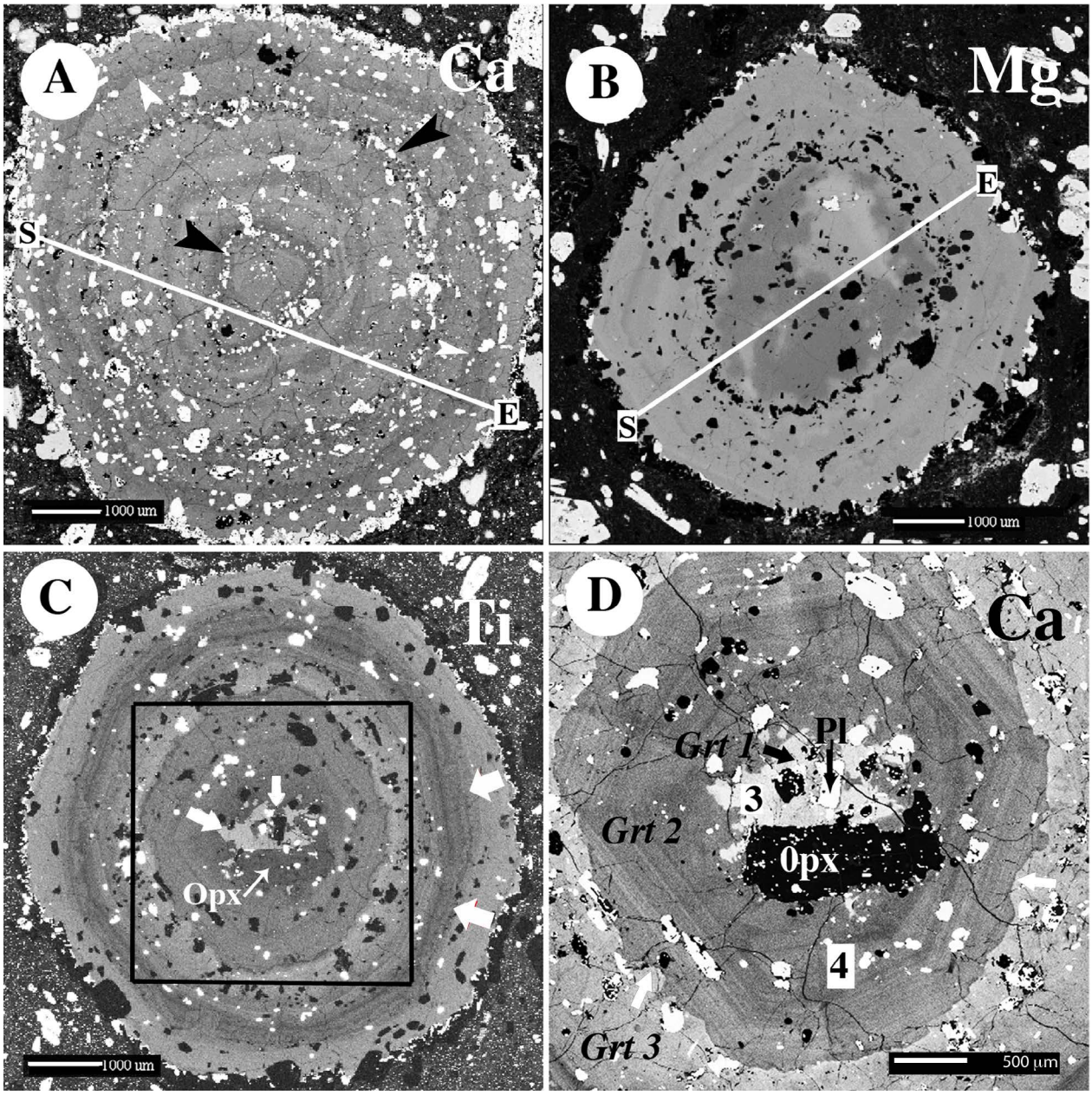

Figure 6: Representative examples of garnet megacrysts. All images are X-ray element maps (Ca, Mg, Ti) in grey scales, adjusted to highlight the differences in composition from one ring to another. Lighter grey represents higher and darker grey lower concentrations for a selected element; the relative intensity scales are different for each map. Numbered spots in white squares refer to garnet analyses in Table 6. Cross-sections labelled SE in panels [A] and [B] correspond to line profiles of analyses (S for start, E for end) given in Figure 8. [A] Ca X-ray image of a common garnet type. Two concentric rings (black arrows) richer in plagioclase inclusions (white) suggest the existence of periods of more rapid growth of the host-garnet, while the scalloped limit in the outer ring (white arrows) underlines an inconspicuous dissolution episode. Note the narrowness of the plagioclase reaction-rim. [B] Mg X-ray image of a rounded garnet megacryst. Regular circular zoning in the outer ring (light grey) testifies for continuous garnet growth without major resorption episodes. Plagioclase inclusions (black) outline the core (dark grey). The light grey pool inside the core is interpreted as evidence of inward corrosion by the Mg-richer external ring. [C] : Ti X-ray image of one of the composite garnets cited in the text. In the outer ring, a slight oscillatory zoning (white arrows) clearly shows the euhedral character of the growing faces. Black arrows outline the corrosion of the central nucleus. [D] Ca X-ray image of the boxed area in Figure 7C. Mineral abbreviations after Whitney and Evans [2010]. The strongly corroded central nucleus (Opx+ Grt 1+ Pl) is overgrown by a euhedral, oscillatory zoned rind (Grt 2). These well-faceted layers (25 to 150 microns wide) are then sharply truncated by a dissolution surface (white arrows) and mantled by a Ca-richer garnet (Grt 3).

Table 6: Representative major element analyses of garnet crystals. n.d. = not detected (below detection limit). Cations based on 12 oxygens (apfu). Comments on occurrence: 1–2: garnet megacryst shown in Figure 10; 3–4: garnet megacryst shown in Figure 6D; 5: euhedral garnet shown in Figure 2B; 6–7: garnet from the garnetite aggregate shown in Figure 5F; 8–9: garnets associated with brown hornblende shown in Figure 2D and Figure 3D; 10–11: composite garnet shown in Figure 9A; 12: metamorphic garnet shown in Figure 3B.

	1	2	3	4	5	6	7	8	9	10	11	12
	Core	Rim	Core	Mantle	Rim	Core	Rim			Core	Rim	Core
SiO_2	37.14	37.73	37.15	37.84	38.49	38.90	37.86	38.00	37.85	38.31	37.66	37.17
TiO_2	0.25	0.28	0.34	0.14	0.21	0.13	0.06	0.22	0.22	0.02	0.59	0.08
Al_2O_3	20.77	20.61	20.20	21.19	21.87	21.59	21.37	20.98	21.20	21.62	21.01	21.30
FeO	31.80	30.05	29.20	29.79	27.43	29.98	30.11	29.88	31.05	30.95	30.68	35.77
MnO	1.87	2.48	2.55	2.88	0.98	0.73	2.54	1.93	1.63	1.66	1.56	1.10
MgO	3.90	4.74	4.01	4.71	6.42	8.67	4.81	5.24	5.48	6.25	4.29	4.20
CaO	4.64	4.73	5.49	4.46	5.24	1.13	4.41	4.90	2.96	2.25	5.11	1.42
Na_2O	0.03	n.d.	0.05	0.02	0.01	0.04	n.d.	0.01	0.01	n.d.	0.04	0.01
K_2O	n.d.	0.02	0.02	0.00	0.03	n.d.	0.02	0.05	n.d.	0.01	n.d.	n.d.
Total	100.40	100.64	99.00	101.03	100.71	101.17	101.17	101.21	100.38	101.05	100.94	101.05
Cations based on 12 oxygens.												
Si	2.96	2.98	2.98	2.97	2.98	2.99	2.97	2.97	2.98	2.98	2.96	2.95
Al iv	0.04	0.02	0.02	0.03	0.02	0.01	0.03	0.03	0.02	0.02	0.04	0.05
Al vi	1.91	1.90	1.90	1.94	1.98	1.94	1.95	1.91	1.95	1.97	1.92	1.95
Ti	0.01	0.02	0.02	0.01	0.01	0.01	0.00	0.01	0.01	0.00	0.03	0.00
Fe_3^+	0.07	0.08	0.07	0.05	0.01	0.04	0.05	0.07	0.03	0.02	0.04	0.04
Fe_2^+	2.05	1.91	1.89	1.91	1.77	1.88	1.93	1.88	2.01	1.99	1.98	2.34
Mn	0.13	0.17	0.17	0.19	0.06	0.05	0.17	0.13	0.11	0.11	0.10	0.07
Mg	0.46	0.56	0.48	0.55	0.74	0.99	0.56	0.61	0.64	0.73	0.50	0.50
Ca	0.40	0.40	0.47	0.38	0.43	0.09	0.37	0.41	0.25	0.19	0.43	0.12
Total	8.03	8.02	8.01	8.02	8.01	8.01	8.02	8.02	8.01	8.01	8.01	8.03
Almandine	66.69	62.27	62.11	62.37	58.4	62.11	62.93	61.34	66.42	65.74	64.96	76.55
Andradite	3.37	3.85	3.46	2.48	0.44	2.11	2.30	3.54	1.62	1.22	2.21	1.92
Grossular	10.02	9.58	12.43	10.16	14.06	0.99	10.18	10.26	6.74	5.07	12.34	2.17
Pyrope	15.65	18.73	16.16	18.56	24.87	33.20	18.92	20.55	21.57	24.32	16.99	16.85
Spessartine	4.26	5.57	5.84	6.44	2.15	1.58	5.68	4.30	3.64	3.66	3.51	2.51

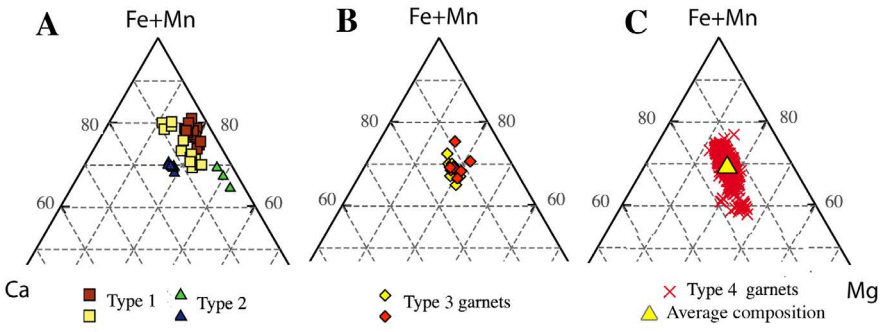

Figure 7: Composition of the different garnet types plotted in terms of (Fe+Mn)-Ca-Mg (all Fe as Fe_2^+). [A] Type 1 metamorphic garnets (red squares = cores, yellow squares = rims) and Type 2 garnets in garnetites (green triangles = cores, blue triangles = rims). [B] Type 3 garnets = minor magmatic garnet associated with brown hornblende, either in reaction rims around metasedimentary enclaves (red diamonds) or in discrete hornblende phenocrysts or hornblende-plagioclase clots (yellow diamonds). [C] Type 4 garnet megacrysts. The cluster of red crosses aggregates 774 spot analyses (four profiles + individual analyses); large yellow triangle denotes the average garnet composition.

Table 7: Analyses in the large crystallised melt pools shielded in the garnet megacryst shown in Figure 10. n.d. = not detected (below detection limit). Comments on occurrence : 1–3 : spot analyses of feldspars; cations based on 32 oxygens (apfu). 4–6 : mean compositions of the crystallised melt obtained with a defocalised beam (20 × 20 microns).

	1	2	3	4	5	6
SiO_2	66.25	61.85	64.42	71.61	76.52	71.71
TiO_2	0.04	0.04	0.01	0.02	0.06	0.12
Al_2O_3	19.00	23.03	21.24	16.15	13.79	15.94
FeOt	0.25	0.74	0.22	0.74	0.29	0.60
MnO	n.d.	0.04	n.d.	0.03	0.03	0.03
MgO	n.d.	0.43	n.d.	0.13	0.04	0.04
CaO	0.84	5.59	3.06	2.92	2.65	3.21
Na_2O	2.97	6.60	6.19	3.83	3.22	4.19
K_2O	11.68	1.25	4.82	3.89	3.20	2.73
Total	101.03	99.58	99.96	99.32	99.80	98.57
Cations based on 32 oxygens						
Si	11.94	11.06	11.52			
Ti	0.01	0.01	0.00			
Al	4.04	4.85	4.48			
Fe	0.04	0.11	0.03			
Mn	0.00	0.01	0.00			
Mg	0.00	0.12	0.00			
Ca	0.16	1.07	0.59			
Na	1.04	2.29	2.15			
K	2.69	0.29	1.10			
Total	19.92	19.81	19.86			
An	4.2	30.5	15.8			
Ab	25.6	61.4	54.5			
Or	70.2	8.1	29.7			

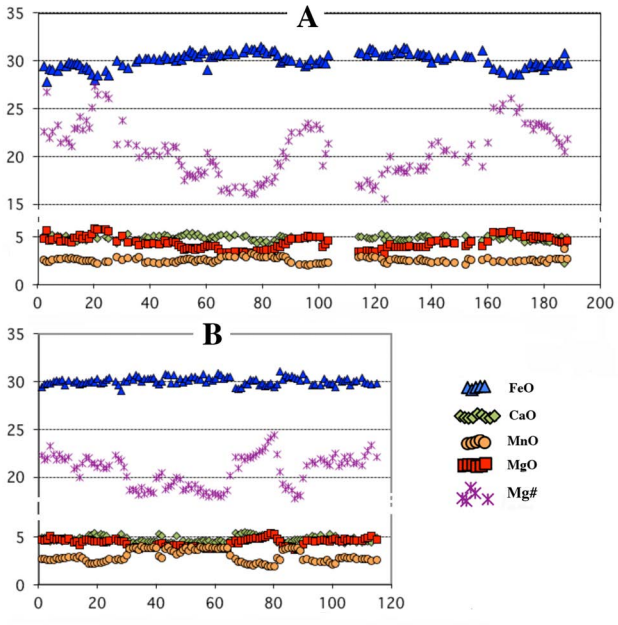

Figure 8: Compositional profiles from rim to rim across the two garnet megacrysts shown in Figure 6A and 6B. Spacing between analysis points for both profiles is 50 microns, except where interrupted by cracks or inclusions. Analyses plotted as weight % oxides : FeO = blue triangles , MgO = red squares, CaO = green diamonds, MnO = orange circles, Mg# = purple crosses (Mg# = Mg/Fe+Mg in the structural formulae, all Fe calculated as Fe_2^+).

cise nature of the melt pools. If it seems clear that this melt was quartz-saturated, its other properties are unknown. However, the occurrence of Ti-magnetite suggests more oxidising conditions than usual, as ilmenite is by far the most common oxide included in garnet. To conclude, because orthopyroxene shows some evidence of corrosion (Figure 10C), it seems likely that this discontinuity reflects a significant resorption episode rather than a simple break during garnet growth. In other words, this suggests that these melt pools differed significantly from the main batch of magma from which garnet crystallised.

7 Thermobarometric data

According to Harangi et al. [2001], primary garnets and coexisting minerals in lavas from the northern Pannonian Basin crystallised at high pressures (0.7–1.2 GPa) and temperatures (800–940 °C). Temperatures were estimated by using the amphibole-plagioclase and garnet-biotite thermometers in garnet-bearing dacites, and pressure estimates were inferred from phase equilibrium relationships established experimentally on a dacitic composition by Green [1992]. Extracting pressure-temperature (PT) estimates from the mineral compositions actually measured in the Breziny andesite was not plausible because the main phases (garnet-amphibole-plagioclase-orthopyroxene) are not strictly contemporaneous, and so global equilibrium conditions were probably never fulfilled. For this reason, PT conditions inferred for the formation of garnet and amphiboles will be treated separately.

7.1 Estimation of PT conditions of garnet formation

Theoretically, several mineral phase equilibria permit constraint of the temperatures of crystallisation of garnet and its related inclusions. They involve Fe-Mn (garnet-ilmenite) and Fe-Mg (garnet-biotite, garnet-orthopyroxene) exchange-reactions, as well as the Al-in-orthopyroxene "thermobarometer". These conventional thermobarometric calculations were done with the program "GTB 2.1" [Spear and Kohn 1999], that gathers several calibrations for each equilibrium. Estimates obtained from the hornblende-garnet thermometer have been discarded due to obvious non-equilibrium between the two phases.

Using ilmenite trapped in garnet would, at least theoretically, permit the calculation of temperatures at the time of garnet growth. Ilmenite inclusions indeed are probably shielded from fast Fe-Mn re-equilibration by the comparatively low Fe-Mn diffusion in garnet [Pownceby et al. 1991]. In fact, variations in spessartine content as low as 0.5 % lead to differences in temperature up to 200 °C, and the whole set of results ranges from 625 to 990 °C. The application of the various calibrations of the biotite-garnet thermometer to biotite inclusions in garnet also produces the same wide range of temperatures, with differences up to 220 °C for the same mineral pair from one calibration to another. As a whole, the data set covers a range from 600 to 1060 °C at a reference pressure of 0.8 GPa. Most values, however, are comprised between 770 and 990 °C, with two clusters of unknown significance around 785 and 900 °C. As the question of estimation of ferric/ferrous iron ratio is far less important for orthopyroxene than for biotite, the garnet-orthopyroxene thermometer is presumably more reliable than the biotite one. At the reference pressure of 0.8 GPa, results from the whole set of calibrations and coexisting mineral pairs still range from 600 to 900 °C. Most of them however are higher than 830 °C, with the most elevated values, given in particular by the calibrations of Sen and Bhattacharya [1984] and Lee and Ganguly [1988], reaching 880 °C.

The Al-in-Opx thermobarometer, based on the P-T-X dependance of Al_2O_3 in orthopyroxene coexisting with garnet [Harley and Green 1982; Harley 1984] is subject to very large uncertainties and therefore of little practical use. It is indeed highly sensitive to small differences in Al_2O_3 content in orthopyroxene and leads to widely scattered results. Differences in Al_2O_3 content up to 2.5 wt% may arise in the same grain (Figure 5B), leading to differences in pressure as high as 0.5 GPa at a reference temperature of 800 °C. Accordingly, results obtained from this thermobarometer have been discarded.

Pressure estimates may be theoretically derived by using the garnet-orthopyroxene-silica-plagioclase (GOSP) barometer [Newton and Perkins 1982]. Commonly used in granulite terrains, this barometer requires that quartz be present to give significant pressure estimates. In the absence of quartz, it defines an upper pressure limit [Seifert and Schumacher 1986; Kriegsman and Hensen 1998]. Because garnet and orthopyroxene grains used for calculations have more than 60 and 50 % almandine and ferrosilite components respectively, it is assumed that pressures determined from Fe-calibrations should be more accurate. Accordingly, the Fe-calibrations of Bohlen et al. [1983], Perkins and Chipera [1985], and Moecher et al. [1988] were used, and at a reference temperature of 900 °C, maximum pressure estimates are comprised between 0.7 and 0.9 GPa.

7.2 Comparison with independent thermobarometric estimations

7.2.1 *Amphibole thermobarometry*

Theoretically, estimates of the temperature range of crystallisation of amphiboles may be obtained directly from their chemical composition [Ridolfi et al. 2010]. Brown hornblendes, whatever their localisation, give results grouped between 910 and 920 °C whereas the green hornblendes indicate significantly higher temperatures (975 °C). These estimates have been duplicated using the plagioclase-hornblende geothermometer of Holland and Blundy [1994]. In the absence of quartz phenocrysts, the thermometer designed for silica-undersaturated rocks was used. Based on the equilibrium edenite + albite = richterite + anorthite [Holland and Blundy 1994], it is almost insensitive to pressure. Estimates at 1 GPa are in broad agreement with the results based on amphibole chemistry alone. The highest values, indeed, are obtained for the glomeroporphyric aggregates of plagioclase + green hornblende, with a significant drop in temperature from core (980–1000 °C) to rim (900 °C). Plagioclase-brown hornblende associations from the garnet-bearing clots dispersed in the lava give mean values around 900 °C, whereas those issued from the reaction-rims surrounding the metasedimentary enclaves give significantly higher results (T_{mean} = 970 °C). These values broadly correspond to the upper limit of hornblende stability in andesitic melts as deduced from experiments: depending on the degree of water-saturation, amphibole is stable in an acid andesitic melt up to 950 ± 20 °C [Eggler 1972].

Due to the pressure dependance of water-solubility in magmas, amphibole is unstable at shallow depths and a minimum pressure of about 0.15 GPa (5–6 km depth) is required for its stabilisation. But this phase is likely to crystallise from an upper-crustal storage chamber to mantle depths, and it is therefore critical to assess, even approximately, pressure conditions of crystallisation of both types of amphiboles. The barometer designed by Ridolfi et al. [2010] suggests that the whole collection of amphiboles crystallised at pressures around 0.4–0.5 GPa. As this type of barometer, only considering amphibole composition, has been shown to often yield untenable pressure estimates [Erdmann et al. 2014], these values must be considered with extreme caution. In spite of the lack of the required coexisting mineral assemblage, the Al-in-amphibole barometry [Schmidt 1992] has been applied for comparison. Although these results have no absolute value, they record higher pressures from 0.6 to 0.9 GPa. Whether amphibole actually crystallised in reservoirs located in the middle crust (16 to 20 km), as suggested by the method of Ridolfi et al. [2010], or deeper in the lower crust remains an open question. However, it must be noticed that both types of calculation suggest that green horn-

blendes originated from a slightly deeper level than the brown ones.

7.2.2 *Two-oxides Fe-Ti thermometry*

For explosively erupted and rapidly cooled volcanic samples it is commonly accepted that the Fe-Ti oxides compositions reflect the conditions in the magma storage region prior to eruption [e.g. Venezky and Rutherford 1997]. Fe-Ti oxides, however, re-equilibrate on cooling much more readily than do silicates [Buddington and Lindsley 1964] and for this reason, this geothermometer requires reconstructing the compositions of the primary phases in order to provide valuable data. Ilmenite and magnetite grains on Figure 5C attest that the Breziny andesite was not quenched and that some subsolidus re-equilibration occurred. Both phases exhibit exsolution lamellae (respectively reduction- and oxidation-exsolution lamellae) that document intra-oxide re-equilibration during cooling. This process theoretically permits both phases to maintain internal equilibrium, so there is little or no exchange between them during cooling [Bohlen and Lindsley 1987]. Reintegrating the intergrowths thus gives the original compositions of the adjacent grains, and permits the calculation of a temperature that confidently reflects the last stage of equilibration. Using the Quartz-Ulvospinel-Ilmenite-Fayalite (QUILF) algorithm [Andersen et al. 1993], and after reintegration of the exsolutions, compositions of the magnetite-ilmenite pairs yield to a maximum temperature of 880–890 °C. However, one cannot exclude the possibility that the oxides initially re-equilibrated on cooling through inter-oxide exchange of iron and titanium, thus leading to higher fossil temperatures.

7.3 Conclusion on thermobarometry

Thermal conditions of garnet crystallisation are not precisely constrained. Orthopyroxene-garnet thermometry suggests that temperatures probably ranged between 850 and 900 °C, in line with values obtained by amphibole and two-oxide thermometry. However, higher values cannot be excluded. On the other hand, low-T conditions such as those suggested by Rottier et al. [2019], down to 750 °C, seem unlikely. Pressure conditions are not better known, as two problems severely limit the use of the ternary assemblage Grt-Opx-Pl for barometric purpose: 1) equilibrium conditions are not fully guaranteed for the different types of associations investigated; 2) above all, calculations strongly depend on Al content in orthopyroxene, and variations inside the same grain (Figure 5B) lead to differences in pressure as high as 0.5 GPa. Given these uncertainties, deriving an accurate and robust estimate of the PT conditions of garnet crystallisation is illusive unless a realistic Al content of orthopyroxene is estimated. Garnet probably crystallised at pressures that were not significantly lower than 0.8 GPa, the limit experimentally demonstrated for Ca-rich garnets in andesitic liquids [Alonso-Perez et al. 2009]. On the other hand, based on experimentally established phase relations, the absence of clinopyroxene fixes an upper limit for garnet crystallisation. With this understanding, a precise value cannot be proposed and the depth interval of crystallisation of garnet megacrysts still remains unconstrained. Due to the lack of any confident pressure data about amphibole crystallisation, the same conclusion holds for Type 3 garnets associated with brown hornblende.

8 Petrogenetic inferences from zircon

Zircon grains included in garnet have been dated *in situ* using LA-ICP-MS in four garnet-bearing lavas from western Slovakia, including the SK8 andesite [Bouloton and Paquette 2014]. In this lava, 27 spots were measured on 17 grains and yielded, in a Tera-Wasserburg diagram, a lower intercept age at 13.3 $\pm$ 0.2 Ma. These zircons lack obvious inherited cores, suggesting that the magma was undersaturated in Zr at the source. As a consequence, zircon is assumed to have nucleated homogeneously from the melt, saturation being implicitly reached by a drop in temperature. Alternatively, these grains could correspond to older zircons completely reset by dissolution-reprecipitation, a process that also implies a decrease in temperature.

As zircon is mantled in garnet, its minimum crystallisation temperature may normally be estimated from that of its host. Summing up the thermobarometric data available, the garnet - orthopyroxene - plagioclase association is assumed to have crystallised at a minimum temperature of 850 °C. On the other hand, the zircon saturation temperature (T_{Zr}) estimated for the bulk andesite, according to Watson and Harrison [1983], is equal to 750 °C. It is likely that T_{Zr} calculated from bulk-rock compositions, if the magma was undersaturated in Zr, provides minimum estimates of temperature [Miller et al. 2003]. However, the difference is so large that it clearly indicates that the bulk andesitic melt was too depleted in Zr to reach saturation at major-mineral liquidus temperatures. The same conclusion holds for apatite inclusions, for which the calculated saturation temperature [Harrison and Watson 1983] is even lower (< 600 °C). Thus, one cannot escape the question of the origin of the included zircon. An elegant solution would be that zircon, due to local saturation, was grown in a specific boundary layer close to the growing garnet megacrysts and was subsequently enclosed. This hypothesis supposes a combination of rapid garnet growth with slow diffusion of zirconium away from the advancing garnet interface, leading to the formation of a chemical layer in which zircon solubility is lower than in the surrounding liquid [Green and Watson 1982; Bacon 1989]. This mech-

anism seems likely but does not explain the presence, although rare, of free zircons in the groundmass (Figure 5D). It is likely then, that zircon, in order to attain saturation, was grown from a melt of significantly different, more evolved composition, than the bulk andesite. Watson [1979] indeed determined that, in peraluminous haplogranitic liquids, less than 100 ppm Zr is required to saturate the melt and crystallise zircon. Later changes in magma chemistry due to magma mixing and/or assimilation account for free zircons in the melt that were almost totally dissolved, whereas zircons shielded into garnets were preserved. Lastly, it must be stressed that in absence of any obvious inherited core, the investigated zircon grains are assumed to have most probably crystallised spontaneously through homogeneous nucleation from a melt.

9 Origin and significance of almandine-rich volcanic garnet: facts and assumptions

Experimental data and geological observations demonstrate that garnet, due to its very wide solution series, may nucleate and grow in almost any lava, including phonolites and tephrites. It may also crystallise from the top to the bottom of the volcanic plumbing system, from post-magmatic fumarolic crystals grown in cavities and fractures [Miyashiro 1955; Moscati and Johnson 2014] to phenocrysts crystallised at sub-crustal depths in underplated mafic magmas [Day et al. 1992; Bach et al. 2012]. More precisely, high T–high P crystallisation experiments have shown that almandine-rich garnet is a liquidus or near-liquidus phase at depth in any calc-alkaline melt from tholeitic to rhyolitic composition [Green and Ringwood 1968; Green 1972; Carroll and Wyllie 1990; Green 1992]. On the other hand, fluid-absent melting experiments carried out on various crustal compositions demonstrated that garnet is the most common phase that grows as a result of incongruent reactions during partial melting of the lower crust [Vielzeuf and Schmidt 2001].

Accordingly, high-pressure garnet megacrysts from calc-alkaline volcanics may, *a priori*, equally well represent phenocrysts precipitated from a cooling magma or reaction products grown during a melting event. More precisely, garnets may have nucleated and grown in any of the three following types of melt: 1) a dacitic or andesitic liquid derived by fractional crystallisation of a mantle-derived melt; 2) a purely crustal melt of anatectic origin; 3) a hybrid melt resulting from the complete mixing of these two components. Moreover, the possibility exists that some garnet cores represent residues from digested metamorphic material, either extracted from the melted source or collected from garnet-bearing wall-rocks at a higher-level. Summing up, any given garnet found in silicic to intermediate lavas could at one extreme be primary and magmatic, and at the other be an unmodified pre-anatectic metamorphic grain. Between these two extremes would lie newly grown peritectic crystals—either issued from melting of a crustal protolith or xenoliths collected during ascent—and any kind of xenocrysts partially modified by reaction with the magma [Clarke 2007].

9.1 General considerations on volcanic garnet chemistry

As any magmatic phase, garnet chemistry depends primarily on magma composition and to a lesser extent on pressure and temperature conditions. Critical compositional parameters are Al, Mn and Ca contents, Mg/Fe ratio, and a_{SiO_2}, $f(H_2O)$ and $f(O_2)$. The role of Al on garnet stability was clearly highlighted for instance by Conrad et al. [1988]: in coupled melting experiments at 1 GPa, they obtained garnet above the solidus in a graywacke composition with 2.8 % normative corundum but did not observe garnet for similar conditions in a dacite with 3.3 % normative diopside. Besides, Green [1976; 1977] and Clemens and Wall [1981; 1984; 1988] among others have delineated the effects of Fe/Fe+Mg, Ca, and Mn on the composition of near-liquidus garnet. Ca and Mn contents, in particular, have been shown to be sensitive to pressure-temperature conditions: Ca content in garnet coexisting with rhyolitic to andesitic liquids increases with increasing pressure [Green and Ringwood 1972; Green 1977; 1992; Patiño Douce 1996], whereas a higher Mn content stabilises garnet at shallower depths [Green 1977].

Summarising, depending on the peraluminous (corundum-normative) vs. metaluminous (diopside-normative) character of their host-lavas, one may as a first approximation distinguish two main types of volcanic garnets. Garnets from peraluminous magmas of S-type affinity are characterised by a low Ca content (CaO < 3 wt%) and are believed to crystallise at crustal depths in magmas derived from a crustal, possibly metasedimentary, source. The most typical example of such peraluminous lavas is undoubtedly the El Hoyazo dacite, in southeastern Spain, a garnet- and cordierite-bearing lava that was initially described as an "erupted migmatite" [Zeck 1970]. In contrast, garnets from the dacites and andesites of Whangarei Heads (Northland Arc, New Zealand) provide good examples of the second type, characteristic of metaluminous lavas of I-type affinity. These are Ca-rich garnets (CaO up to 9 wt%) assumed to have grown at subcrustal depths from a mafic liquid, either mantle-derived [Day et al. 1992] or subduction-related [Bach et al. 2012]. Between these two end-members lie garnets characterised by intermediate CaO contents (5–7 wt%), such as those from the Carpathian volcanic arc. However, the Carpathian garnets are not unique, as volcanic garnets with a similar composition are known elsewhere in the world, for instance in rhyolites and dacites from Setouchi, Japan

[Kawabata and Takafuji 2005] or those from Canterbury, New Zealand [Barley 1987] as well as in some andesites from Trinity Peninsula, Antarctica [Hamer and Moyes 1982].

Compared to volcanic garnets from Whangarei Heads, those from Breziny should not be rigorously referred to as Ca-rich garnets. They clearly show intermediate compositions between these garnets and those from typical peraluminous lavas. However, for the sake of simplicity, they are still described as Ca-rich garnets in the next sections, but the two types of garnets—Ca-poor and Ca-rich—will be discussed separately.

9.2 Origin of Ca-poor garnet: Xenocrystic, pre-anatectic or peritectic?

Ca-poor garnets are always mantled by a Ca-rich magmatic overgrowth compositionally identical to the megacrysts dispersed in the lava, attesting that they interacted with a melt of roughly similar nature. Depending on the type of interaction—from complete immersion into the melt to infiltration along grain boundaries—the width of the Ca-rich overgrowth varies largely (compare Figure 5E and Figure 9A). But its significance is always the same: it expresses the adaptation of the mineral to a new environment. Once mantled by a magmatic overgrowth in equilibrium with the enclosing melt, the garnet core then acts as an armoured relic and will persist until the compositional gradient is completely erased by diffusion. The survival of tiny Ca-poor nuclei in the garnetites, however, demonstrates that complete homogenisation was not achieved even at magmatic temperatures. Owing to time constraints, re-equilibration processes may commonly be incomplete and xenocrystic or restitic garnet cores are thus able to survive inside garnet megacrysts. These cores are all the more obvious as the chemical contrast with their overgrowth is strong, as is the case for the Ca-poor ones. But one may keep in mind, in this regard, that any potential pre-anatectic garnet core with a grossular content approximately analogous to that of its magmatic overgrowth should easily go unnoticed. This possibility can in no way be ruled out since garnets which, in the metamorphic domain, characterise Ca-rich basic rocks of the amphibolite and granulite facies [Popov 1983] actually exhibit the same major element chemistry than the Ca-rich magmatic megacrysts in SK8.

9.2.1 *Is there any evidence of contamination and assimilation of xenocrystic garnet?*

Geochemical studies suggest that mantle derived magmas traversing the continental crust may undergo considerable crustal contamination. Occurrence of garnet xenocrysts, either primary or modified by reaction with the magma, would support such a process. According to definitions given in the introduction of this study, xenocrysts correspond to accidental inclusions scavenged by the magma from the wall-rocks at any level above the primary source region. In this paper, contamination and assimilation are used in the sense of Clarke [2007], that is, contamination is the process by which a foreign material is added to the magma and changes its bulk composition, and assimilation eliminates the original physical evidence that contamination took place. Coexistence of phenocrystic and xenocrystic garnets in lavas has been reported worldwide [Hamer and Moyes 1982; Clemens and Wall 1984; Kawabata and Takafuji 2005]. This coexistence has even been taken to suggest that assimilation of garnet-bearing wall-rocks may cause the crystallisation of garnet phenocrysts [Clemens and Wall 1984].

In this regard, the Ca-poor core of the composite megacryst shown in Figure 9, that plausibly reflects derivation from the neighbouring melt-depleted metasedimentary enclave described in Section *4.3.1* (Figure 3A), illustrates this point. This garnet exemplifies a contamination—assimilation process "caught in the act"—but its precise significance must be discussed in further detail. PT data collected from the magmatic reaction-rim of the metasedimentary enclave suggest that it was scavenged from the lowermost crust [Didier et al. 2015]. However, it was shown that this enclave is not a restite for its enclosing lava. Partial melting indeed is assumed to be Variscan in age [Didier et al. 2015], and this xenolith corresponds in fact to a fragment of a refractory layer, only superficially affected by the Miocene magmatic event. Although it is a significant witness of the lower crust implied in the Carpathian volcanism it does not strictly belong to the genuine magma system. It corresponds to a resister, and the core of the composite garnet expelled from this enclave is a resister too. It thus represents a compelling example of inherited, pre-anatectic garnet of deep-seated origin. Ca-poor cores of Type 3 garnets occurring in the reaction rims of the metasedimentary enclaves share a broadly similar history and are most likely representative of pre-anatectic garnets.

Garnets in hornblende-plagioclase aggregates and garnet inclusions in brown hornblende phenocrysts, for their part, are not clearly distinguishable from Type 4 garnet megacrysts in ternary diagrams (Figure 7). Whether they record a more advanced stage of transformation than the garnets described just above, or suffered a basically different history, is currently unknown. Bearing in mind the high temperatures and protracted time scales associated with deep crustal anatexis, metamorphic garnets may suffer dissolution-reprecipitation processes making them unidentifiable, due to their compositional similarity with early cotectic liquidus phases [Villaros et al. 2009; Taylor and Stevens 2010]. On the other hand, the common presence of biotite inclusions in brown hornblende suggests that amphibole crystallisation is related to a melting process involving a biotite-bearing protolith. Accordingly,

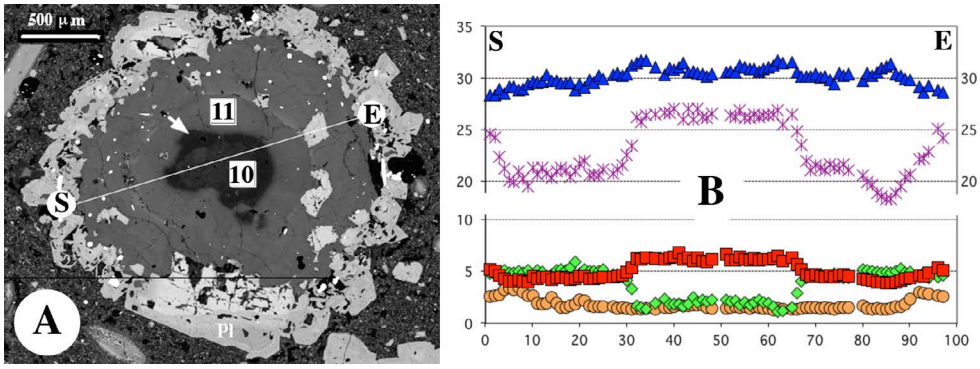

Figure 9: Details about the composite garnet shown in Figure 3E. [A] Ca X-ray image showing the metamorphic CaO-poor core (dark grey) and its Ca-richer magmatic overgrowth (pale grey). The garnet is surrounded by a large granular reaction-rim almost exclusively composed of plagioclase (white). Note the idiomorphic character of plagioclase in contact with the groundmass. Numbers in white boxes refer to garnet analyses in Table 6. [B] The compositional profile shows the strong depletion in CaO and the corresponding enrichment in MgO of the metamorphic core relative to the magmatic overgrowth. Symbols as in Figure 8.

some new garnet could have been generated through this melting reaction. Due to the lack of reliable pressure data relative to hornblende crystallisation, the existence of high-level garnet xenocrysts, collected in the middle- or upper-crust, cannot be demonstrated. In summary, no convincing example of garnet xenocryst has been found, and mineralogical evidence of crustal contamination of the andesitic magma during its ascent is currently missing.

9.2.2 *Is there evidence of any other restitic garnet?*

By definition, restitic material consists of solid remnants of the source rocks but also encompasses peritectic minerals, the solid by-products of incongruent melting reactions. Clarke [1995], Erdmann et al. [2009], and Dorais et al. [2009] among others have outlined the difficulty of recognising peritectic minerals in plutonic environments. This task is much more arduous in lavas, because any significant textural information about the melting event is lost. Significant information could only be found in partially molten, garnet-bearing, restitic enclaves, if any. In this respect, the origin of the Ca-poor garnet nuclei in garnetites (Figure 5F) is questionable. From a simple descriptive point of view, garnetites are aggregates of garnet microphenocrysts and represent something like small cumulative nodules. The chemical composition of these microcrysts indicates that they have grown, for the most part, in the same melt as the garnet megacrysts. Garnet cores, by contrast, have a very different composition, implying a different origin. Based on experimental evidence, Hensen and Green [1973] considered that garnet with such a low Ca content (CaO < 2 wt%) could never have been in equilibrium with a hypersthene + diopside normative liquid, a liquid akin with their present-day enclosing lava. Ca-depleted nuclei in garnetites may thus correspond to: 1) mineral fragments like the pre-anatectic, inherited garnets previously described, or to: 2) peritectic minerals, the solid by-products of an incongruent melting reaction. No one argument allows at present the distinction between the two above possibilities. However, since the composition of these nuclei is slightly different from that of the inherited Type 1 metamorphic garnets, but quite similar to that of synthetic garnets grown in partial melting experiments of peraluminous protoliths (see Section 9.3.2), the second hypothesis is tentatively favoured. The garnet nuclei from the garnetites are thus interpreted to reflect the melting reaction of a specific layer of metapelitic composition, prior to changes in magma chemistry leading to the crystallication of the Ca-richer garnet.

9.3 Origin of Ca-rich garnet: Cotectic or peritectic?

As noted previously, high-pressure liquidus garnets may equally well represent phenocrysts precipitated from a cooling magma or reaction products grown during a melting event. In other terms, Ca-rich garnet can nucleate and grow from a cooling melt according to the cotectic reaction L → Opx+Pl+Grt. Alternatively, it can be produced through an incongruent melting reaction of the type Bt+Pl±Hb±Qtz → Grt+Opx+melt. The uncertainty around the nature of garnet—peritectic vs. cotectic—is far from anecdotal, as it conveys critical information about the conditions of magma generation. Cotectic garnet indicates that the silicate melt reached saturation in garnet through changes in T (cooling) or X (assimilation/mixing), or both. On the other hand, peritectic garnet suggests that garnet resulted from a melt-producing fluid-absent reaction, most probably in response to rising temperature.

In the absence of partially molten garnet-bearing xenoliths, no direct information on melting conditions is available and the possibly peritectic nature of gar-

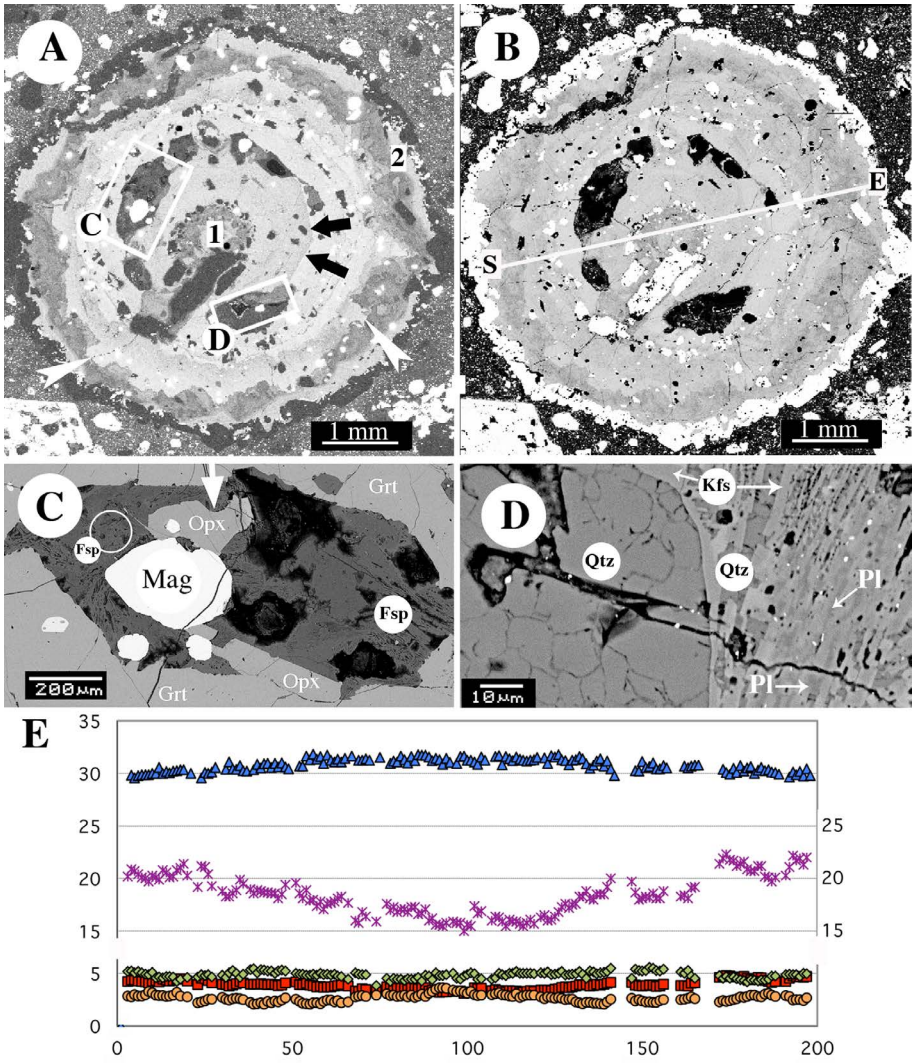

Figure 10: Details about the crystallised melt hollows cited in the text. [A] Ti X-Ray map of the subhedral, complexly zoned garnet megacryst. White rectangles (lettered C and D) outline large pools of crystallised melt, up to 2 mm long, that define a discontinuous ring discordant on the euhedral growth zoning (white arrows). Numbers in white boxes refer to garnet analyses in Table 6. [B] Ca X-Ray map of the same garnet. S-E line refers to the profile shown in Figure 8E. [C] BSE image of a crystallised melt hollow, showing large crystals of orthopyroxene and magnetite in a groundmass partly composed of acicular feldspars. Opx crystal is slightly embayed (arrow), suggestive of magmatic corrosion. The Ti-magnetite crystal is certainly too large, relative to the total volume of the hollow, for having crystallised after trapping of this melt pool by the growing garnet. Mineral abbreviations after Whitney and Evans [2010]. [D] Close-up view of the crystallised groundmass, composed of acicular laths of feldspar interspersed with quartz. Plagioclase microliths have a systematic overgrowth of alkali feldspar, most probably precipitated as thin rims on earlier-formed crystals when the residual melt became sufficiently enriched in K, near the solidus temperature. The large quartz grain is characterised by slightly curvilinear faces that attest of some dissolution by reaction with the enclosing melt. The significance of the "mosaic" texture visible in the crystal is unknown. E: Corresponding compositional zoning profile following S-E. Spacing between analysis points is 30 microns, except where interrupted by cracks or inclusions. Symbols as in Figure 8.

net cannot be ascertained on a textural basis. The only way to tackle this topic is to compare natural data (mineral assemblages and phase compositions) with the results of HT-HP experiments conducted under realistic pressures (~1GPa). In other words, the aim is to find a melt able to crystallise garnet with a composition akin to that of SK8, with about 5 wt% CaO and 4.5 wt% MgO. However, because of the large number of interrelated intensive and extensive variables, phase relations in molten systems are too complicated for drawing any definitive conclusion from such a simple comparative exercise. Besides P, T, $X(H_2O)$, and $f(O_2)$, compositional parameters such as Fe/Mg or Ca/Na ratios indeed control, through the different behaviours

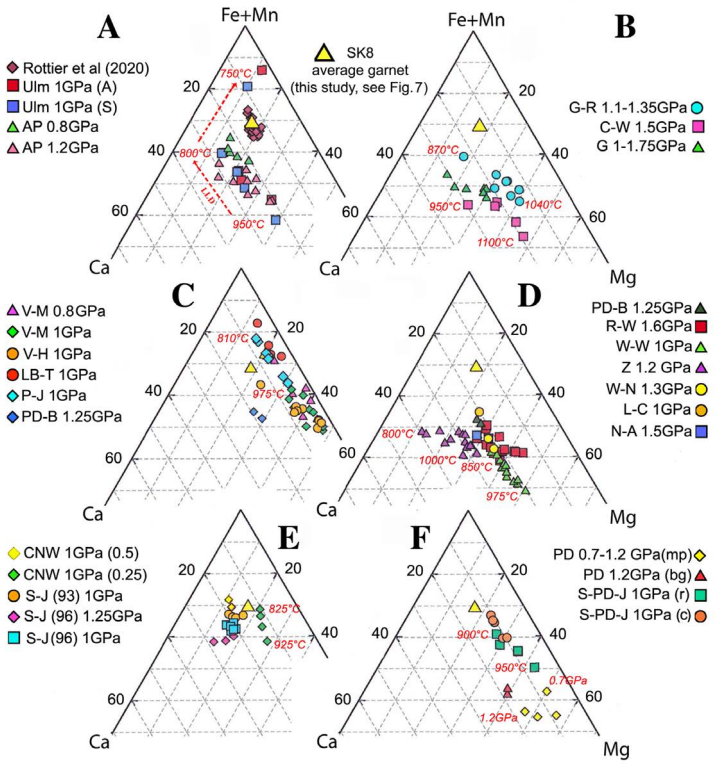

Figure 11: (Fe+Mn)-Ca-Mg ternary plots showing compositions of various synthetic garnets obtained in HT-HP experiments. All Fe as FeO. Pressures and temperatures are those corresponding to occurrence of garnets shown in the diagrams ; the whole set of experimental conditions cited in the following papers may be larger. Composition of average Breziny garnet is reported for comparison in any diagram (yellow triangle). [A] Most recent and detailed crystallisation experiments. AP = Alonso-Perez et al. [2009]: on a synthetic andesite, 0.8–1.2 GPa (green and red triangles respectively), 850 to 1000 °C, 4 to 8 wt% H_2O; Ulm = Ulmer et al. [2018]: two series of fractional crystallisation experiments starting from a high-Mg andesite (blue squares) and a high-Mg basalt (red squares), 1 GPa, 950 to 750 °C. Dotted line = liquid line of descent. Garnet analyses from Rottier et al. [2019] are reported for comparison (brown diamonds). [B] First crystallisation experiments to determine phase equilibria within the crystal + liquid interval. G-R = Green and Ringwood [1972]: rhyodacite, 1.14 to 1.8 GPa, 900 to 1040 °C, 2–5 wt% H_2O; G = Green [1992]: dacite, 1 to 1.75 GPa, 850–950 °C, 3–10 wt% H_2O; C-W = Carroll and Wyllie [1990]: tonalite, 1.5 GPa, 950 to 1100 °C, 2.4–2.6 wt% H_2O added. [C] Fluid-absent melting experiments on aluminous crustal protoliths. V-H = Vielzeuf and Holloway [1988]: natural metapelite,1 GPa, 875 up to 1050 °C, rims; V-M = Vielzeuf and Montel [1994]: natural metagraywacke, 0.8 and 1 GPa, 855–1000 °C; LB-T = Le Breton and Thompson [1988]: synthetic pelitic composition (mixture of natural minerals), 1 GPa, 850 °C ; P-J = Pickering and Johnston [1998]: natural two-mica metapelite, 1 GPa, 812 to 975 °C; PD-B = Patiño Douce and Beard [1995]: synthetic biotite gneiss (mixture of natural minerals), 1.25 GPa, 930–960 °C. [D] Fluid-absent melting experiments on mafic protoliths. PD-B = Patiño Douce and Beard [1995]: synthetic quartz amphibolite (mixture of natural minerals), 1.25 GPa, 930–960 °C; W-W = Wolf and Wyllie [1993]: natural low-K calcic amphibolite, 1 GPa, 850–990 °C ; R-W = Rapp and Watson [1995]: four different amphibolites, 1.6 GPa, 1000 to 1100 °C ; Z = Zhang et al. [2013]: synthetic amphibolite, 1.2 GPa, 800–1000 °C ; L-C = López and Castro [2001]: MORB-derived amphibolite, 1 GPA, 900 °C. Results obtained from fluid-deficient melting experiments (5 wt% water added) are also shown. W-N = Winther [1991]: synthetic low-K tholeite, 1.3 Gpa, 900–1000 °C; N-A = Nakajima and Arima [1998]: low-K tholeite, 1.5 GPa, 1000 °C. [E] Crystallisation and melting experiments that best approximate the Breziny garnet composition. CNW = Conrad et al. [1988]: crystallisation from a synthetic glass representing a S-type peraluminous metagraywacke, 1 GPa, 725–925 °C, fluid-deficient conditions (0.25–0.5 $X_{\mathrm{vap}_{H_2O}}$). SJ(93) = Skjerlie and Johnston [1993]: fluid-absent melting of an F-rich tonalitic gneiss, 1 GPa, 875–950 °C; SJ(96) = Skjerlie and Johnston [1996]: fluid-absent melting of a metavolcanoclastic rock (slightly metaluminous natural paragneiss), 1 and 1.25 GPa, 850–925°C. [F] Experiments on hybrid assemblages. PD = Patiño Douce [1995]: melting and crystallisation experiments on sandwich materials (metapelite and biotite gneiss + high-Al olivine tholeite), 0.7–1.2 GPa, 1000 °C S-PD-J = Skjerlie et al. [1993]: fluid-absent melting of a layered (pelite + tonalite) assemblage, 1 GPa, 900–950 °C, r and c = rim and core compositions of garnet respectively.

of the various phases involved, melting and/or crystallising reactions. Ultimately, they control the assemblages, proportions, and compositions of solid phases, along with the melt composition. Bearing in mind these limitations, the following discussion will try to: 1) examine whether or not the primary Grt-Opx-Pl assemblage that characterises SK8 may actually crystallise from a mantle-derived melt, as supposed by Rottier et al. [2019]; 2) evaluate the possible role of a crustal melting event; 3) evaluate which type of crustal protolith might have been involved.

9.3.1 *Experimental constraints on liquids derived from a mantle melt*

Pioneering studies [Green and Ringwood 1968; Green 1972] demonstrated that garnet is a high-pressure liquidus or near-liquidus phase in calc-alkaline melts from acid to basic compositions, and outlined the major role of water on the relevant phase equilibria. Dissolved H_2O significantly influences both the crystallisation sequence (amphibole in water-rich and pyroxene in water-poor melts) and the abundance and composition of minerals. Basically, higher water content in the melt suppresses plagioclase and leads to crystallisation of amphibole and garnet. More precisely, experiments on a natural island-arc andesite (SiO_2 = 60 wt%) in the pressure interval 0.9–3.6 GPa, under anhydrous conditions and with various added water contents (2, 5, and 10 wt%), clearly delineated the stability fields of the different solid assemblages coexisting with a melt [Green 1972]. A significant conclusion from this study is that orthopyroxene, whatever the experimental conditions, was never found contrary to the other expectable mafic phases (garnet-hornblende-clinopyroxene). The question thus arises whether and how a mantle-derived melt is able to crystallise a Grt-Opx-Pl assemblage.

Similar HP-HT experiments [Green 1992] on a more evolved lava (SiO_2 = 64.5 wt%) showed that orthopyroxene coexists with garnet only for a very small pressure range (0.05–0.15 GPa) above the incoming of garnet in garnet-seeded runs. Indeed, with 5 wt% added water, a very narrow stability field is expected for the assemblage Grt+Hb+Opx+Cpx+Pl+melt around 900 °C and 0.8 GPa, but the simple anhydrous assemblage Grt-Pl-Opx was not observed in any run. Compositions of the garnets obtained in these various experiments, expressed in terms of (Fe+Mn)-Ca-Mg components, are shown in Figure 11B.

More recently, a series of 25 equilibrium experiments has been conducted [Alonso-Perez et al. 2009] in order to mimic the behavior of a mantle-derived melt in the depth range of 25–40 km, a melt that is either underplated at the base of the continental crust or ponded within the lower crust. These experiments cover the crystallisation interval of a synthetic andesitic composition at conditions ranging from 0.8 to 1.2 GPa, 800 to 1000 °C and variable H_2O contents (added H_2O contents of 4, 6, and 8 wt%) under oxidising conditions (fO_2 between QFM and Ni-NiO). The starting compositions (54.8–53.2 wt% SiO_2, A/CNK = 0.94) correspond to an "experimental" liquid (basaltic andesite) previously obtained from fractional crystallisation experiments at 1 GPa-1020 °C starting from a natural, hydrous picrobasalt. All derivative liquids produced in this study are Qz-normative and evolve to peraluminous compositions, covering the complete range from basaltic andesite to rhyolite. At high pressure (1.2 GPa), garnet is a major phase over the entire range of conditions (800–1000 °C, 4–8 wt% H_2O) and coexists either with clinopyroxene, amphibole and plagioclase, depending on T and water content. At lower pressure (0.8 GPa) and water contents of 6–8 wt%, garnet, amphibole and plagioclase are stable from 800 to 900 °C. Significantly, orthopyroxene was reported in only one run (1.2 GPa, 900 °C, 4 wt% H_2O), together with garnet, plagioclase, clinopyroxene, ilmenite and melt. Once again, the simple anhydrous assemblage Grt-Pl-Opx was not recognised in any run.

Finally, thorough additional information may be found in a recent paper by Ulmer et al. [2018]. These authors conducted several series of equilibrium and fractional crystallisation experiments at 1 GPa under various fO_2 and fH_2O conditions to evaluate and quantify the liquid lines of descent of calc-alkaline to tholeiitic, hydrous, subduction-related primary mantle magmas. Two different starting compositions representing variable mantle source extraction conditions were used, a high-Mg basalt and a high-Mg basaltic andesite, respectively. Fractional crystallisation experiments were performed over restricted temperature steps of mostly 30 °C and 50 °C below 1000 °C and they covered, for both starting compositions, the whole temperature range from 1230 °C (the liquidus temperature of the andesite) to 750 °C. Under oxidised conditions, the fractional crystallisation series evolved to dacite and finally rhyolite, reaching silica contents of nearly 75 wt % at 750 °C. Crystallisation from andesite to rhyolite is controlled by amphibole+garnet+plagioclase fractionation, resulting in a similar line of descent for both initial starting compositions below 900 °C. In both series, garnet joins the fractionating assemblage at the same temperature (950 °C), where it coexists with plagioclase and amphibole. But whatever the experimental conditions, it never co-crystallises with orthopyroxene, that instead forms the liquidus phase in basaltic andesite and disappears at 1050 °C in the fractional crystallisation experiments, in a peritectic reaction forming amphibole. Compositions of the garnets obtained in these crystallisation experiments, and the corresponding liquid line of descent, are shown in Figure 11A.

A major petrological observation is that garnet crystallised from such evolved melts in association with hornblende and plagioclase, never coexists with or-

thopyroxene. In summary, it seems highly difficult—if not impossible—that the former Grt-Opx-Pl assemblage evidenced in SK8 crystallised from a mantle-derived melt.

9.3.2 *Melting experiments and crustally-derived melts*

The anhydrous character of the Grt-Opx-Pl assemblage suggests that crystallisation began at relatively high-T and/or under strongly H_2O undersaturated conditions. Apart from the large crystals of plagioclase and orthopyroxene, garnet inclusions also comprise rounded crystals of biotite and plagioclase, but inclusions of sillimanite or quartz have never been found. This suggests that a fluid-absent melting reaction of the type: Bt+Pl+Qtz → Grt+Opx+melt could have occurred, in which the quartz reactant was entirely consumed and a few biotite crystals preserved. Accordingly, only experiments conducted on water-deficient systems were considered, either corresponding to fluid-absent or water-fluxed melting.

Compositions investigated experimentally include strongly peraluminous metapelites, peraluminous to mildly metaluminous metagreywackes, and more deeply metaluminous rocks such as tonalitic gneisses and basaltic amphibolites. To the first order, fluid-absent melting of the deep crust (P ~ 1 GPa) is likely to produce a broadly granitic melt in equilibrium with peritectic garnet in the whole range of common compositions, from metapelites to metabasites. The compositions of synthetic garnets produced in a number of melting experiments are shown in Figure 11, and compared with the average composition of SK8 garnets, in order to assess what type of crustal protolith might represent a likely source.

Garnet and orthopyroxene are the two major mafic phases formed by incongruent melting of biotite-rich protoliths (metagraywackes) in the pressure range considered [Vielzeuf and Montel 1994; Gardien et al. 1995; Patiño Douce and Beard 1995]. However, garnet compositions vary largely depending on the nature of the starting material and experimental conditions. For instance, garnets grown during partial melting of a natural peraluminous metagraywacke [Vielzeuf and Montel 1994] have significantly lower Ca contents than the SK8 megacrysts (Figure 11C). On the other hand, experiments on a synthetic material slightly less aluminous but significantly Ca-richer (2.1 against 1.64 wt% CaO) lead to higher Ca contents in garnet [Patiño Douce and Beard 1995]. As the PT conditions are almost the same, this suggests that the bulk Ca content has a major influence on garnet composition. Slightly metaluminous paragneisses and tonalitic gneisses (muscovite-free, biotite and/or amphibole-bearing rocks) also are suitable sources for giving rise to garnet and orthopyroxene assemblages, with garnet compositions approaching the SK8 ones (Figure 11E). On the other hand, fluid-absent melting of amphibolitic and/or basaltic compositions produce garnets that are clearly too rich in Ca and Mg (Figure 11D). However, the lack of melting experiments with added water does not permit to definitely exclude the possibility of a significant contribution of the mafic lower crust.

Indeed, melting experiments conducted with various contents of added water widen the field of possibilities. Specifically, experiments by Conrad et al. [1988] on a peraluminous greywacke composition at 1 GPa, with a_{H_2O} ranging from 0.25 to 1, are highly informative. At a_{H_2O} = 0.25 and under reducing conditions (oxygen fugacity close to the QFM buffer), they show the coexistence of Opx+Grt+Pl+Ilm+melt, with a grossular content in synthetic garnet close to the average value measured in SK8 garnets (Figure 11E). Moreover, results obtained at a_{H_2O} = 0.5 suggest that a smaller increase in water activity could generate a garnet matching those in SK8. However, the sequence of crystallisation is different from that deduced in SK8 from petrographic investigation. At a_{H_2O} = 0.25, garnet is the liquidus phase at 950 °C, joined by orthopyroxene and plagioclase+ilmenite at 925 °C. It is later followed by quartz 50 °C lower. At 925 °C, the proportion of glass (with calculated H_2O content = 4 wt%) is important (> 80 wt%); this water-undersaturated melt is rhyolitic (SiO_2 = 69 wt%) and strongly corundum-normative (C = 1.97). The crystalline cargo (> 15%) comprises nearly equivalent quantities of orthopyroxene and plagioclase, that together represent half the content of garnet. The main difference with the natural phases in SK8 is the higher Al_2O_3 content of orthopyroxene (8 wt% vs. 5 wt% at most). Due to the well-known tendency of this mineral to grow very fast in experimental conditions (especially from glasses, as in these experiments) and thus to be frequently out of equilibrium leading to excess Al_2O_3 contents, it is not clear whether this discrepancy is significant or not. However, a real problem remains with ilmenite and apatite, that clearly predate garnet in SK8 while they crystallise later in these experiments. Apatite in particular appears up to 150 °C below the liquidus, presumabely due to the very strong peraluminous character of the experimental melt.

Summarising, available melting experiments show that the primary anhydrous association Grt-Opx-Pl documented in SK8 may be generated through fluid-absent or water-fluxed melting in the lower crust. Immature metasediments or volcanoclastic formations, as well as tonalitic gneisses are suitable candidates for source materials. Even though the natural crystallisation sequence is not matched in these experiments, nor the precise compositions of garnet and orthopyroxene, the peritectic nature of the Ca-rich garnet-orthopyroxene association appears as a plausible hypothesis.

9.3.3 *Ca-rich garnet: The peritectic dilemma*

As demonstrated by HT-HP crystallisation experiments, the assemblage Grt-Opx-Pl is unknown in felsic liquids derived from a melt of pure mantle origin. On the other hand, this association is common in fluid-absent or fluid-deficient melting experiments conducted at pressure conditions akin to those of the lower crust on various biotite-bearing compositions, from peraluminous metapelites to tonalitic gneisses. Basically, by comparison with experimental results, it would be tempting to conclude that garnet megacrysts in SK8 are the solid by-product of a melting reaction of the type Bt+Pl+Qtz → Grt+Opx+melt.

If so, garnet would represent a direct mineralogical witness of crustal involvement in andesite magmagenesis and further attention must be paid in this hypothesis to the noritic core of the composite garnet illustrated in Figure 6D. This core might represent: 1) a residue directly inherited from the lower crust, or 2) a rock fragment from a Miocene, upper crustal crystallised magma chamber reactivated during a younger magma injection. In the absence of contradictory evidence, the idiomorphic character of plagioclase (Figure 6D) rather supports the second hypothesis. However, a lot of granulitic xenoliths have been described in Pliocene alkali basalts from Hungary [Embey-Isztin et al. 2003]. Most of them are mafic meta-igneous rocks, among which garnet-rich lithologies are common, but meta-sedimentary granulite xenoliths, characterised by abundant plagioclase and garnet together with subordinate orthopyroxene, have also been identified [Embey-Isztin et al. 2003]. So, the possibility that this noritic core represents a witness of the Pre-Tertiary, possibly Variscan, granulitic lower crust cannot be excluded.

Whatever the real nature of this core, petrological reasoning alone leads to the conclusion that the primary felsic garnet-bearing melt may actually be generated from a noritic protolith. Minerals at the liquidus of a primary liquid indeed set limits on the mineralogy of the residue left in the source after extraction [Myers and Johnston 1996]. For instance, compositions of the early-crystallised, near-liquidus phenocrysts in S-type volcanic rocks have been shown to likely mimic the compositions of their residual and peritectic counterparts [Clemens and Wall 1981]. In other words, any magma that had been in equilibrium with garnet as a restite phase in the source region would indeed be saturated in garnet and would probably remain saturated during its ascent to lower pressures, at least for some time [Clarke 1995]. Even if this melt segregates efficiently, it is believed to be a strong candidate for crystallising just below the liquidus garnet of almost the same composition. In this case, garnet would correspond to a cotectic magmatic mineral.

On the other hand, generation of peritectic garnet at a given pressure implies a rise in temperature, and such a thermal evolution is at odds with the growth conditions inferred from zircons shielded in garnet. These zircons are assumed to have crystallised or recrystallised at decreasing temperature (see Section 8). In these conditions, it is highly difficult to consider that garnet megacrysts, that subsequently enclosed and shielded zircon grains, are peritectic garnets grown in response to rising temperature. Crystallisation of the host garnet phase along a decreasing temperature path, as with its inclusions, appears more likely. Then, the only way to generate a peritectic garnet would be by decompression melting accompanied by a gentle drop in temperature. Even though such a PT path permits, in theory, to cross down the multivariant field of the fluid-absent melting reaction Bt+Qtz+Pl → Grt+Opx+Melt+Kfs [Vielzeuf and Montel 1994], this melting scenario is a matter of conjecture. A geologically reasonable model must take into account the geodynamic regional context of lithospheric thinning and correlated mantle decompression, that necessarily implies significant heating of the lower crust. In these conditions, one can hardly escape a two-step scenario, where the thermally-induced peraluminous crustal melt—with its cargo of peritectic nuclei of garnet and orthopyroxene—would slightly ascend, pond to a higher level in the crust, and then give rise by cooling to the growing garnet megacrysts. In this case, the formal distinction between peritectic and cotectic phases in natural lavas is merely semantic: garnet and orthopyroxene antecrysts in SK8 could equally well be seen as peritectic minerals nucleated during the melting event or cotectic minerals grown subsequently during storage in a deep-seated reservoir.

9.4 Nucleation and growth of garnet: Inferring a plausible scenario

9.4.1 *Melting in the lower crust*

Melting of crustal rocks occurs in a number of different ways that largely depend on source mineralogy and the fluid-regime during the high-temperature event. It is now widely admitted that a pervasive free fluid phase is unlikely to exist beneath the uppermost few km of crust [Yardley and Valley 1997]. Rather, melting in the lower crust is triggered by the breakdown of hydrous minerals, micas and amphiboles; these fluid-absent reactions give rise to H_2O-undersaturated melts and to anhydrous solid residues [Vielzeuf and Holloway 1988, and references therein]. At temperatures of 800–900 °C, any rock containing mica or amphibole will begin to melt incongruently, and depending on the P-T-X conditions, garnet will occur, or not, among the peritectic products of the melting reaction.

Fluid-dominated processes in the deep crust are expected to be rare and localised in extent. However, it is theoretically possible that fluid-present melting occurred locally around mantle-derived basaltic magmas emplaced in the lower crust. According to Annen et al.

[2006], during basalt crystallisation at depth, the H_2O concentration can reach a sufficiently high level to become saturated, resulting in exsolution. For low residual melt fractions in the basalt, saturation occurs if the parent basalt has more than 1 wt% H_2O. If so, exsolved volatiles can possibly flux the overlying crust and induce further melting in the vicinity. In this case, the water-saturated melting process begins with a vapour-present eutectic reaction and ends when no more water is available, a situation that implies two major consequences: 1) the quartzo-feldspathic fraction of the crustal protolith is the main contributor to the melt; 2) no peritectic garnet is formed. Finally, felsic melts produced in the deep crust, whatever their origin, are likely to be mingled/mixed with the mantle-derived magmas responsible for the thermal anomaly and the crustal melting event. As a consequence, magmas produced and stored in the MASH zone should probably correspond in most cases to complex mixtures of crustal melts with their cargo of restitic crystals, and more or less fractionated melts of mantle origin, carrying early-grown orthocrysts.

9.4.2 *A possible scenario for the genesis of Breziny garnet megacrysts*

Petrographic observations and *in situ* U-Pb dating of included zircons clearly demonstrate that garnet megacrysts are igneous in origin. Owing to their size—garnet is the largest crystalline phase in the lava—and their zoning patterns, it is inferred that garnet megacrysts were "slowly" grown in some local magma accumulation. Textural evidence further demonstrates that garnet crystallised from a melt whose composition was evolving with time. Zoning patterns record these changes, outlined in particular by dissolution surfaces that reflect large-scale disturbances of the crystallising system (Figure 6 and Figure 10). On the other hand, it is quite clear that all phenocrystic phases present in the SK8 andesite (amphibole, plagioclase, garnet, orthopyroxene) are not strictly contemporaneous and do not constitute a global equilibrium assemblage. Specifically, brown hornblende post-dates garnet in the crystallisation sequence. Resorbed garnet inclusions in amphibole phenocrysts are common (Figure 2D), and the quasi-absence of the reverse relation (brown hornblende inclusions in garnet) argues against the actual co-crystallisation of both minerals. Furthermore, the common presence of biotite inclusions in brown hornblende strongly suggests that amphibole crystallisation is related to a melting process involving a biotite-bearing protolith. The depth and timing of this event however, are unconstrained.

In contrast, orthopyroxene, which is exceedingly rare as a phenocryst, forms frequent inclusions in garnet (Figure 2E). These inclusions, along with plagioclase inclusions, are present from core to rim of the garnet and also, occasionally, in its external reaction rim, thereby implying that garnet growth took place entirely in a melt pool that was also saturated in the two other phases. It is thus likely that the Grt-Opx-Pl association constitutes, together with a melt, an early-stage equilibrium assemblage. Brown hornblende crystallised in a second step, in the blocky coronas that surround the metasedimentary enclaves and in the reaction-rims of garnet megacrysts. The Grt-Opx-Pl association probably crystallised at higher-T and/or under more strongly H_2O-undersaturated conditions than those prevailing for a typical hornblende andesite. Higher temperatures and relatively dryer conditions indeed favour the crystallisation of orthopyroxene over hornblende. Whether brown hornblende crystallised from the same magma pool as orthopyroxene, due to an increase in a_{H_2O}, or was grown elsewhere in the magmatic system, is currently unknown. As already described, green hornblende phenocrysts are never in contact with garnet. For this reason, their depth of crystallisation cannot be assessed, nor their introduction in the present-day magma dated. In any case, garnet megacrysts in SK8 clearly appear as antecrysts, likely grown in a magma different from the present-day bulk lava.

Available experimental HT-HP data suggest that the primary anhydrous assemblage Grt-Opx-Pl could result from the fluid-absent melting of an immature metasedimentary protolith or from a tonalitic gneiss, producing a more or less peraluminous liquid of broadly rhyolitic composition. However, oxygen isotope data presented by Harangi et al. [2001] suggest a more complex history, involving a mixing event between a crustal melt and a fractionated melt of deeper origin. Bulk analysis of the Breziny garnet provided a $\delta^{18}O$ value relative to SMOW of 6.6 per mil (‰), that suggests a two-component mixing between a mantle-derived magma and crustal material with a relatively low $\delta^{18}O$ value [Harangi et al. 2001]. The reality of this mixing event is supported by a simple petrographic observation, namely the occurrence of apatite inclusions in garnet. The high solubility of apatite in peraluminous liquids [Pichavant et al. 1992] precludes its early precipitation from a purely anatectic melt and this firmly suggests that apatite inclusions crystallised from a less evolved liquid. A change in melt composition occurring very early in the magma system history is thus inferred. This leads to a more complex scenario, where the anatectic melt, transporting garnet and orthopyroxene peritectic nuclei, is extracted from the partially molten rock, stored in a lower-crustal reservoir and immediately mixed with a more mafic magma of deeper origin. Apatite would precipitate from this hybrid melt, and garnet megacrysts, though nucleated in the rhyolitic crustal melt, would in fact be growing in this new magma of probable dacitic composition.

A slightly different scenario may also account for the whole set of observations. It implies a fluid-present melting event and the selective assimilation of this haplogranitic crustal melt by a fractionated melt

of mantle origin. Garnet nucleation and growth, in this case, would directly occur in the hybrid melt. This scenario is consistent with the classic assumption that admixture of a peraluminous material to a mafic magma favours garnet crystallisation, in accordance with the mechanism invoked by Green [1992]. Mixing indeed decreases the normative diopside/hypersthene ratio of the mafic melt and shifts the bulk composition to lower normative diopside and higher normative quartz, allowing crystallisation of garnet at lower pressure than in a metaluminous, more mafic composition [Green 1992]. Experiments conducted by Patiño Douce [1995] on hybrid compositions (50 % basalt and 50 % metapelite) at 1000 °C under various pressures (0.5 to 1.5 GPa) confirm the possibility of garnet crystallisation at high pressure in such mixed melts. Interestingly, strongly peraluminous felsic melts in equilibrium with noritic cumulates (Pl+Opx+Grt) were produced at 0.7 and 1 GPa. However, compositions of both garnet and orthopyroxene synthetic phases are significantly different from those observed in SK8. Moreover, although this scenario in which garnet directly nucleated and grew from the hybrid melt appears *a priori* much simpler, it should be stressed that it does not account for all the data. In particular, crystallising apatite in a strongly peraluminous liquid remains problematic. On the other hand, the search for possible occurrence of relict cores of peritectic origin inside garnet megacrysts would be alleviated. In this respect, it should be remembered that Ca-depleted garnet cores in garnetites were assumed to reflect the fluid-absent melting reaction of a metapelitic component, prior to changes in magma chemistry leading to the crystallisation of their Ca-richer garnet overgrowth. Magma mixing would explain readily why and how such peritectic garnet cores survived as mantled relics. In a closed system, peritectic garnet should suffer back-reaction with the melt during cooling and be reversed by dissolution during magma solidification. However, in an open-system, where the bulk composition is modified by mixing with a different melt, peritectic garnet will tend to chemically re-equilibrate with the evolving magma through crystallisation of an overgrowth and will survive as a mantled core. In the fluid-absent melting scenario, the Ca-poor and Mg-rich garnet cores from the garnetites could record the first stage of a continuous prograde melting event, involving less and less fusible crustal lithologies, from peraluminous two-mica metapelites at 750–800 °C to metaluminous compositions at 900 °C or higher temperatures.

Strictly speaking, neither of the two petrogenetic scenarios is supported by more circumstantial evidence, and whether garnet megacrysts nucleated in a purely crustal melt or directly in a hybrid liquid remains an open question. Both types of garnet nuclei may coexist in SK8, and the only fact indicated by the thermal history of included zircon is that these nuclei subsequently grew in a cooling magma reservoir. Zoning patterns show that all garnet megacrysts however, do not necessarily share the same history. Garnets likely grew from different liquids existing in different places, and possibly at different times, in the magma system. However, the peritectic nature of a few garnet cores, at least, among the whole set of garnet megacrysts is currently not demonstrated. By default, it is thus considered that garnet megacrysts nucleated and grew directly from a hybrid melt. This assumption is in global agreement with the origin proposed by Harangi et al. [2007] for volcanic garnets of the western Carpathian arc on the basis of trace element geochemistry and isotopic arguments. According to these authors, mixing of mafic magmas with silicic melts issued from the metasedimentary lower crust would indeed result in relatively Al-rich hybrid dacitic magmas from which almandine could crystallise at high pressure [Harangi et al. 2007].

9.5 Outstanding issues

Mineralogical information gained from the Breziny andesite confirms the above geochemical scenario, but the nature of the petrologic processes actually operative in the deep crust is still questionable. As indicated by experimental results, almandine-rich garnets broadly similar in composition to SK8 megacrysts may be the solid by-products of melting of immature metagreywackes and/or tonalitic gneisses (Figure 11E). However, at present, any proof of this assumption is missing. Moreover, it is worth noting that in a fluid-absent melting scenario, the absence of any quartz inclusion in garnet seriously questions the nature of the crustal protolith involved. Experiments show that synthetic garnets produced through fluid-absent melting of a metasedimentary material are in general characterised by abundant quartz inclusions. As fluid-absent melting of a mafic protolith seems, on the other hand, inconsistent with the composition of SK8 garnet, the debate about garnet origin still remains open. Once the main petrogenetic characteristics of the Breziny lava are known, a more detailed investigation would be necessary to derive a precise history of garnet crystallisation and to better assess the nature of its parental melt. This study should include the following aspects: 1) search for partially molten restitic enclaves, in which textural relations could support the peritectic nature of garnet; 2) a detailed investigation of the different varieties of amphiboles, in order to better constrain their timing and depth of formation; 3) a systematic quest for melt inclusions of sufficient size in garnet, to characterise trapped liquids; 4) trace elements profiles across garnet and its major inclusions of orthopyroxene and plagioclase; 5) *in situ* $\delta^{18}O$ measurements across garnet equatorial sections.

Trace elements profiles coupled with *in situ* $\delta^{18}O$ measurements could help to demonstrate the possible peritectic origin of some garnet cores, indistinguishable on the sole basis of major element chemistry. Theo-

retically, core-to-rim trace-element profiles allow us to distinguish peritectic garnet formed under equilibrium melting conditions from cotectic garnet crystallised from fractionating melts [Dorais and Tubrett 2012]. Oxygen isotope data, for their part, have been proven to be a powerful complement for determining garnet provenance and distinguishing peritectic from cotectic and xenocrystic garnets in granites [Lackey et al. 2011]. Moreover, *in situ* measurements show that garnet faithfully records $\delta^{18}O$ magmatic changes [Lackey et al. 2012] and constitute, through $\delta^{18}O$ zoning patterns, a valuable tool to decipher magma petrogenesis.

The present work has opened challenging questions concerning the minor inclusions of apatite and zircon, namely the conditions of apatite saturation and the actual temperature of crystallisation of zircon. Apatite solubility depends, among others, both on SiO_2 content (it decreases with increasing SiO_2) and A/CNK value (solubility is higher in peraluminous than metaluminous liquids). Early crystallisation of apatite at presumably high temperature, prior to garnet growth, puts narrow limits to melt composition. Concerning zircon, Rottier et al. [2019] estimated its crystallisation temperature, based on the Ti-in content method of Ferry and Watson [2007], to be equal to 763 $\pm$ 19 °C. This value is almost the same than the T_{Zr} saturation temperature (about 750 °C) estimated for the bulk andesite, about 100 °C lower than the minimum temperature suggested by conventional thermometry for garnet crystallisation. So, the question arises to decide if these estimations actually record the temperature of zircon growth or outline a re-equilibration process after cooling from peak temperatures. Clearly, more attention should be paid in the future to apatite and zircon inclusions in order to better assess their conditions of crystallisation, and accordingly, those of their enclosing garnet. In this respect, the recent critical discussion of zircon-saturation thermometry by Clemens et al. [2020], who discuss the problem in the general context of crustal melting and generation of granitic magmas, appears absolutely pivotal.

In any case, conclusions reached from this study cannot be extended as such to other garnet-bearing lavas of the Carpathian Arc. The garnet-plagioclase-hornblende association—without orthopyroxene—well-known in experimental derivative liquids obtained from fractional crystallisation of mantle-derived melts, is indeed common in dacites [Harangi et al. 2001; Bouloton and Paquette 2014]. Otherwise, andesites are known where garnet, hornblende and orthopyroxene define, together with plagioclase, a phenocrystic assemblage in apparent equilibrium [Harangi et al. 2001; Bouloton and Paquette 2014]. Whether this phenocrystic cargo actually corresponds to a total equilibrium assemblage remains uncertain. Finally, it is worth noting that the Breziny dome itself, due to its heterogeneity at the field scale, well illustrates the difficulties in assessing the origin of garnet. Rottier et al. [2019] indeed collected their garnet sample a few km away from the sampling site of this study, and according to these authors, their lava contains about 6 % volume of orthopyroxene phenocrysts. In these conditions, failing to recognise the antecrystic nature of orthopyroxene is easy and this precludes *a priori* any chance of considering garnet otherwise than an orthocryst. Thus, there is little doubt that the ultimate origin of volcanic garnet in calc-alkaline lavas of the Carpathian Arc will remain a subject of debate in the future.

10 Conclusions

The main results of this study can be summarised as follows:

A. On the basis of their mode of occurrence, garnets of the Breziny dome can be divided into four distinct types, that correspond in order of increasing abundance to: 1) metamorphic garnets occurring in lithic fragments of deep-seated origin; 2) aggregated garnets from garnetite lenses; 3) more or less corroded garnet grains in close association with brown hornblende; 4) discrete garnet megacrysts disseminated in the lava.

B. Chemically, garnet megacrysts form a coherent group with homogeneous composition within and between samples. They are almandine-rich and reflect the formula in mol.%: Almandin 61–67 Pyrope 15–25 Grossular 10–15 Spessartine 2–6 Andradite 2–4. In terms of petrogenetically significant components, these megacrysts, on average, contain about 5 wt% CaO and 4.5 wt% MgO. On the other hand, Type 1 metamorphic garnet cores and Type 2 garnet cores from the garnetites are characterised by much lower Ca contents (CaO $\leqslant$ 2 wt%).

C. Texturally, the main point of interest is that mineral inclusions in garnet megacrysts do not match perfectly the phenocryst population of the host rock. Orthopyroxene commonly occurs as inclusions within garnet, whereas it is exceedingly rare as a phenocryst. On the other hand, only one amphibole variety out of the four types recognised shows connection with garnet. In summary, garnet megacrysts in SK8 do not represent cognate orthocrysts, crystals grown from the melt in which they are now found. Detailed mineralogical evidence indicates that they were grown from an evolving orthopyroxene- and plagioclase-bearing melt, presumably rhyolitic or dacitic, therefore significantly different from the present-day hornblende-bearing lava. Garnet megacrysts are in fact antecrysts and, in consequence, they may possibly record distinct paths and histories of growth, depending on their parental magma pool.

This interpretation is in contrast to earlier studies on garnet-bearing rocks of the Carpathian Arc, which all concluded that garnets show compositional links to their host rocks and correspond to common phenocrysts [Brousse et al. 1972; Embey-Isztin et al. 1985; Harangi et al. 2001].

D. X-ray compositional maps and zoning profiles for major elements reveal a complex history and suggest a temporal and/or spatial variability of the magma system over the timespan of garnet growth. Corrugated interfaces indicative of a resorption process, in particular, are believed to reflect large-scale disturbances of the crystallising system, such as recharge, introduction of a fresh batch of magma in the chamber, or contamination, incorporation, and assimilation of crustal material into the magma.

E. From a genetic point of view, no one xenocrystic garnet has been documented, suggesting that contamination of the andesitic magma during its ascent through the middle- and upper-crust, if any, was unrelated to mechanical erosion of the wall-rocks. Occurrence of pre-anatectic garnets, on the other hand, is demonstrated, but these residual minerals issued from the source region are present in very subordinate quantity. The same remark holds for the Ca-poor and Mg-rich nuclei that characterise garnets from the garnetite lenses. These nuclei plausibly correspond to the solid by-products of the fluid-absent, incongruent melting of a broadly metapelitic layer. But the role of this peritectic garnet in terms of global contamination is obviously subordinate and rules out any strong metapelitic contribution to andesite magmagenesis.

F. Assessing the true nature of Ca-rich garnet megacrysts is far from easy. Comparison with available fractional crystallisation experiments precludes the possibility that the early Grt-Opx-Pl assemblage might have been formed by cooling of a genuine mantle-derived melt. By contrast, fluid-absent melting of an immature metasedimentary protolith, for instance, is able to produce this anhydrous assemblage, in equilibrium with a felsic peraluminous melt. On the sole basis of comparison with experimental results, it is thus tempting to conclude that garnet megacrysts are the solid by-product of a melting reaction of the type Bt+Pl+Qtz → Grt+Opx+melt. However, thermal evolution inferred from zircons shielded in garnet is at odds with this model. Zircons indeed lack any obvious inherited core, suggesting that the magma was undersaturated in Zr at the source. For this reason, zircon is assumed to have most probably nucleated homogeneously from the melt by a drop in temperature. In these conditions, it is difficult to consider that garnet megacrysts, that subsequently enclosed and shielded zircon grains, are peritectic garnets grown in response to rising temperature.

G. In order to reconcile the whole set of information, a two-step scenario must be envisaged. The thermally-induced anatectic melt, with its cargo of peritectic nuclei of garnet and orthopyroxene, separates from the rest of the partially-molten protolith, ascends and ponds a little bit higher in the lower crust. Cooling of this magma batch then leads to garnet growth, giving rise to mm- to cm-sized megacrysts. In this case, the formal distinction between peritectic and cotectic garnet appears somewhat immaterial. Alternatively, a slightly different scenario can be proposed, implying a water-saturated melting event and the concomitant assimilation of the resulting haplogranitic crustal melt by the intrusive mantle-derived melt responsible for the thermal anomaly. In this case, the anhydrous primary Grt-Opx-Pl assemblage would crystallise directly from this hybrid magma. Given the current absence of evidence to support the peritectic nature of any garnet megacryst core, the second scenario is presently favoured and garnet megacrysts, by default, are believed to have nucleated and grown by cooling of this crustal- and mantle-derived composite magma.

H. This assumption is in agreement with available $\delta^{18}O$ isotopic data, which support the hypothesis of mixing of mantle-derived mafic magmas with silicic melts issued from the metasedimentary lower crust [Harangi et al. 2007]. From a petrologic point of view, the garnet-orthopyroxene association, whatever its precise meaning, clearly documents this lower crustal contamination history. A better understanding of the processes actually involved would certainly be achieved by clarifying the growth history of garnet through trace elements profiles coupled with *in situ* $\delta^{18}O$ measurements. Otherwise, the present study invalidates the recent proposal [Rottier et al. 2019] that Breziny garnet crystallised at "low" temperatures from an evolved, residual melt derived from fractionation of a primitive magma of mantle origin.

Acknowledgements

This study has greatly benefited in its beginning, some years ago, from stimulating discussions with D. Vielzeuf and C. Pin. Special thanks are due to J. L. Devidal and the late J. M. Henot for their technical assistance during the microprobe and SEM sessions. Fieldwork was supported by the "Service des relations internationales" from the Clermont University. Many thanks are due to D. Hovorka, P. Ivan and S. Meres from Comenius University in Bratislava for their logistic support in Slovakia. P. Boivin is acknowledged for his comments on volcanology and assistance with computer technology. C. Pin critically reviewed a first

draft of the manuscript and greatly improved the writing. Constructive and careful reviews by S. Harangi and R. J. Moscati and helpful comments by A. J. Jeffery are greatly appreciated.

Data availability

All data used in this study are presented in Tables 1, 2, 3, 4, 5, 6 and 7. The author can also provide geological data upon request.

Copyright notice

References

Alonso-Perez, R., O. Müntener, and P. Ulmer (2009). "Igneous garnet and amphibole fractionation in the roots of island arcs: experimental constraints on andesitic liquids". *Contributions to Mineralogy and Petrology* 157.4, pp. 541–558. DOI: 10.1007/s00410-008-0351-8.

Andersen, D. J., D. H. Lindsley, and P. M. Davidson (1993). "QUILF: A pascal program to assess equilibria among FeMgMnTi oxides, pyroxenes, olivine, and quartz". *Computers & Geosciences* 19.9, pp. 1333–1350. DOI: 10.1016/0098-3004(93)90033-2.

Annen, C., J. D. Blundy, and R. S. J. Sparks (2006). "The Genesis of Intermediate and Silicic Magmas in Deep Crustal Hot Zones". *Journal of Petrology* 47.3, pp. 505–539. DOI: 10.1093/petrology/egi084.

Bach, P., I. E. M. Smith, and J. G. Malpas (2012). "The Origin of Garnets in Andesitic Rocks from the Northland Arc, New Zealand, and their Implication for Sub-arc Processes". *Journal of Petrology* 53.6, pp. 1169–1195. DOI: 10.1093/petrology/egs012.

Bacon, C. R. (1989). "Crystallization of accessory phases in magmas by local saturation adjacent to phenocrysts". *Geochimica et Cosmochimica Acta* 53.5, pp. 1055–1066. DOI: 10.1016/0016-7037(89)90210-x.

Barley, M. (1987). "Origin and evolution of mid-Cretaceous, garnet-bearing, intermediate and silicic volcanics from Canterbury, New Zealand". *Journal of Volcanology and Geothermal Research* 32.1-3, pp. 247–267. DOI: 10.1016/0377-0273(87)90047-3.

Bohlen, S. R. and D. H. Lindsley (1987). "Thermometry and Barometry of Igneous and Metamorphic Rocks". *Annual Review of Earth and Planetary Sciences* 15.1, pp. 397–420. DOI: 10.1146/annurev.ea.15.050187.002145.

Bohlen, S. R., V. J. Wall, and A. L. Boettcher (1983). "Experimental investigation and application of garnet granulite equilibria". *Contributions to Mineralogy and Petrology* 83.1-2, pp. 52–61. DOI: 10.1007/bf00373079.

Bouloton, J. and J. Paquette (2014). "In situ U–Pb zircon geochronology of Neogene garnet-bearing lavas from Slovakia (Carpatho-Pannonian region, Central Europe)". *Lithos* 184-187, pp. 17–26. DOI: 10.1016/j.lithos.2013.10.020.

Brousse, R., H. Bizouard, and J. Šalát (1972). "Grenats des andésites et des rhyolites de Slovaquie, origine des grenats dans les séries andésitiques". *Contributions to Mineralogy and Petrology* 35.3, pp. 201–213. DOI: 10.1007/bf00371215.

Buddington, A. F. and D. H. Lindsley (1964). "Iron-Titanium Oxide Minerals and Synthetic Equivalents". *Journal of Petrology* 5.2, pp. 310–357. DOI: 10.1093/petrology/5.2.310.

Carroll, M. R. and P. J. Wyllie (1990). "The system tonalite-H2O at 15 kbar and the genesis of calc-alkaline magmas". *American Mineralogist* 75.3-4, pp. 345–357.

Cashman, K. V., R. S. J. Sparks, and J. D. Blundy (2017). "Vertically extensive and unstable magmatic systems: A unified view of igneous processes". *Science* 355.6331, eaag3055. DOI: 10.1126/science.aag3055.

Chernyshev, I. V., V. Konečný, J. Lexa, V. A. Kovalenker, S. Jeleň, V. A. Lebedev, and Y. V. Goltsman (2013). "K-Ar and Rb-Sr geochronology and evolution of the Štiavnica Stratovolcano (Central Slovakia)". *Geologica Carpathica* 64.4, pp. 327–360. DOI: 10.2478/geoca-2013-0023.

Clarke, D. B. (1995). "Cordierite in felsic igneous rocks: a synthesis". *Mineralogical Magazine* 59.395, pp. 311–325. DOI: 10.1180/minmag.1995.059.395.15.

– (2007). "Assimilation of xenocrysts in granitic magmas: principles, processes, proxies, and problems". *The Canadian Mineralogist* 45.1, pp. 5–30. DOI: 10.2113/gscanmin.45.1.5.

Clemens, J. D., G. Stevens, and S. E. Bryan (2020). "Conditions during the formation of granitic magmas by crustal melting – Hot or cold; drenched, damp or dry?" *Earth-Science Reviews* 200, p. 102982. DOI: 10.1016/j.earscirev.2019.102982.

Clemens, J. D. and V. J. Wall (1981). "Origin and crystallization of some peraluminous (S-type) granitic magmas". *The Canadian Mineralogist* 19.1, pp. 111–131.

– (1984). "Origin and evolution of a peraluminous silicic ignimbrite suite: The Violet Town Volcanics". *Contributions to Mineralogy and Petrology* 88.4, pp. 354–371. DOI: 10.1007/bf00376761.

– (1988). "Controls on the mineralogy of S-type volcanic and plutonic rocks". *Lithos* 21.1, pp. 53–66. DOI: 10.1016/0024-4937(88)90005-9.

Conrad, W. K., I. A. Nicholls, and V. J. Wall (1988). "Water-Saturated and -Undersaturated Melting of Metaluminous and Peraluminous Crustal Compositions at 10 kb: Evidence for the Origin of Silicic Magmas in the Taupo Volcanic Zone, New Zealand, and Other Occurrences". *Journal of Petrology* 29.4, pp. 765–803. doi: 10.1093/petrology/29.4.765.

Crabtree, S. M. and R. A. Lange (2011). "Complex Phenocryst Textures and Zoning Patterns in Andesites and Dacites: Evidence of Degassing-Induced Rapid Crystallization?" *Journal of Petrology* 52.1, pp. 3–38. doi: 10.1093/petrology/egq067.

Day, R. A., T. H. Green, and I. E. M. Smith (1992). "The Origin and Significance of Garnet Phenocrysts and Garnet-Bearing Xenoliths in Miocene Calc-alkaline Volcanics from Northland, New Zealand". *Journal of Petrology* 33.1, pp. 125–161. doi: 10.1093/petrology/33.1.125.

Didier, A., V. Bosse, J. Bouloton, S. Mostefaoui, M. Viala, J. L. Paquette, J. L. Devidal, and R. Duhamel (2015). "NanoSIMS mapping and LA-ICP-MS chemical and U–Th–Pb data in monazite from a xenolith enclosed in andesite (Central Slovakia Volcanic Field)". *Contributions to Mineralogy and Petrology* 170.5-6. doi: 10.1007/s00410-015-1200-1.

Dorais, M. J., T. K. Pett, and M. Tubrett (2009). "Garnetites of the Cardigan Pluton, New Hampshire: Evidence for Peritectic Garnet Entrainment and Implications for Source Rock Compositions". *Journal of Petrology* 50.11, pp. 1993–2016. doi: 10.1093/petrology/egp058.

Dorais, M. J. and M. Tubrett (2012). "Detecting Peritectic Garnet in the Peraluminous Cardigan Pluton, New Hampshire". *Journal of Petrology* 53.2, pp. 299–324. doi: 10.1093/petrology/egr063.

Eggler, D. H. (1972). "Amphibole stability in H2O-undersaturated calc-alkaline melts". *Earth and Planetary Science Letters* 15.1, pp. 28–34. doi: 10.1016/0012-821x(72)90025-8.

Embey-Isztin, A., G. Noske-Fazekas, G. Kurat, and F. Brandstätter (1985). "Genesis of garnets in some magmatic rocks from Hungary". *TMPM Tschermaks Mineralogische und Petrographische Mitteilungen* 34.1, pp. 49–66. doi: 10.1007/bf01082457.

Embey-Isztin, A., H. Downes, P. D. Kempton, G. Dobosi, and M. Thirlwall (2003). "Lower crustal granulite xenoliths from the Pannonian Basin, Hungary. Part 1: mineral chemistry, thermobarometry and petrology". *Contributions to Mineralogy and Petrology* 144.6, pp. 652–670. doi: 10.1007/s00410-002-0421-2.

Erdmann, S., R. A. Jamieson, and M. A. MacDonald (2009). "Evaluating the Origin of Garnet, Cordierite, and Biotite in Granitic Rocks: a Case Study from the South Mountain Batholith, Nova Scotia". *Journal of Petrology* 50.8, pp. 1477–1503. doi: 10.1093/petrology/egp038.

Erdmann, S., C. Martel, M. Pichavant, and A. Kushnir (2014). "Amphibole as an archivist of magmatic crystallization conditions: problems, potential, and implications for inferring magma storage prior to the paroxysmal 2010 eruption of Mount Merapi, Indonesia". *Contributions to Mineralogy and Petrology* 167.6. doi: 10.1007/s00410-014-1016-4.

Fediukova, E. (1975). "Garnets from neovolcanics in Slovalia." *Krystalinikum* 11, pp. 53–62.

Ferry, J. M. and E. B. Watson (2007). "New thermodynamic models and revised calibrations for the Ti-in-zircon and Zr-in-rutile thermometers". *Contributions to Mineralogy and Petrology* 154.4, pp. 429–437. doi: 10.1007/s00410-007-0201-0.

Gardien, V., A. B. Thompson, D. Grujic, and P. Ulmer (1995). "Experimental melting of biotite plagioclase quartz ± muscovite assemblages and implications for crustal melting". *Journal of Geophysical Research: Solid Earth* 100.B8, pp. 15581–15591. doi: 10.1029/95jb00916.

Gill, J. B. (1981). *Orogenic Andesites and Plate Tectonics*. Springer Berlin Heidelberg. isbn: 978-3-540-10666-1. doi: 10.1007/978-3-642-68012-0.

Green, T. H. (1972). "Crystallization of calc-alkaline andesite under controlled high-pressure hydrous conditions". *Contributions to Mineralogy and Petrology* 34.2, pp. 150–166. doi: 10.1007/bf00373770.

– (1976). "Experimental generation of cordierite-or garnet-bearing granitic liquids from a pelitic composition". *Geology* 4.2, p. 85. doi: 10.1130/0091-7613(1976)4<85:egocgg>2.0.co;2.

– (1977). "Garnet in silicic liquids and its possible use as a P-T indicator". *Contributions to Mineralogy and Petrology* 65.1, pp. 59–67. doi: 10.1007/bf00373571.

– (1982). "Anatexis of mafic crust and high pressure crystallization of andesite". *American Society of Mechanical Engineers (Paper)*, pp. 465–487.

– (1992). "Experimental phase equilibrium studies of garnet-bearing I-type volcanics and high-level intrusives from Northland, New Zealand". *Earth and Environmental Science Transactions of the Royal Society of Edinburgh* 83.1-2, pp. 429–438. doi: 10.1017/s0263593300008105.

Green, T. H. and A. E. Ringwood (1968). "Origin of garnet phenocrysts in calc-alkaline rocks". *Contributions to Mineralogy and Petrology* 18.2, pp. 163–174. doi: 10.1007/bf00371807.

– (1972). "Crystallization of garnet-bearing rhyodacite under high-pressure hydrous conditions". *Journal of the Geological Society of Australia* 19.2, pp. 203–212. doi: 10.1080/14400957208527881.

Green, T. H. and E. B. Watson (1982). "Crystallization of apatite in natural magmas under high pressure, hydrous conditions, with particular reference to"Orogenic" rock series". *Contributions to Mineralogy and Petrology* 79.1, pp. 96–105. doi: 10.1007/bf00376966.

Hamer, R. D. and A. B. Moyes (1982). "Composition and origin of garnet from the Antarctic Peninsula Volcanic Group of Trinity Peninsula". *Journal of the Geological Society* 139.6, pp. 713–720. DOI: 10.1144/gsjgs.139.6.0713.

Harangi, S., H. Downes, L. Kósa, C. Szabó, M. F. Thirlwall, P. R. D. Mason, and D. Mattey (2001). "Almandine Garnet in Calc-alkaline Volcanic Rocks of the Northern Pannonian Basin (Eastern–Central Europe): Geochemistry, Petrogenesis and Geodynamic Implications". *Journal of Petrology* 42.10, pp. 1813–1843. DOI: 10.1093/petrology/42.10.1813.

Harangi, S., H. Downes, M. Thirlwall, and K. Gméling (2007). "Geochemistry, Petrogenesis and Geodynamic Relationships of Miocene Calc-alkaline Volcanic Rocks in the Western Carpathian Arc, Eastern Central Europe". *Journal of Petrology* 48.12, pp. 2261–2287. DOI: 10.1093/petrology/egm059.

Harley, S. L. (1984). "An experimental study of the partitioning of Fe and Mg between garnet and orthopyroxene". *Contributions to Mineralogy and Petrology* 86.4, pp. 359–373. DOI: 10.1007/bf01187140.

Harley, S. L. and D. H. Green (1982). "Garnet–orthopyroxene barometry for granulites and peridotites". *Nature* 300.5894, pp. 697–701. DOI: 10.1038/300697a0.

Harrison, T. M. and E. B. Watson (1983). "Kinetics of zircon dissolution and zirconium diffusion in granitic melts of variable water content". *Contributions to Mineralogy and Petrology* 84.1, pp. 66–72. DOI: 10.1007/bf01132331.

Hensen, B. J. and D. H. Green (1973). "Experimental study of the stability of cordierite and garnet in pelitic compositions at high pressures and temperatures". *Contributions to Mineralogy and Petrology* 38.2, pp. 151–166. DOI: 10.1007/bf00373879.

Hildreth, W. and S. Moorbath (1988). "Crustal contributions to arc magmatism in the Andes of Central Chile". *Contributions to Mineralogy and Petrology* 98.4, pp. 455–489. DOI: 10.1007/bf00372365.

Hildreth, W. and C. J. N. Wilson (2007). "Compositional Zoning of the Bishop Tuff". *Journal of Petrology* 48.5, pp. 951–999. DOI: 10.1093/petrology/egm007.

Holland, T. and J. Blundy (1994). "Non-ideal interactions in calcic amphiboles and their bearing on amphibole-plagioclase thermometry". *Contributions to Mineralogy and Petrology* 116.4, pp. 433–447. DOI: 10.1007/bf00310910.

Irving, A. J. and F. A. Frey (1978). "Distribution of trace elements between garnet megacrysts and host volcanic liquids of kimberlitic to rhyolitic composition". *Geochimica et Cosmochimica Acta* 42.6, pp. 771–787. DOI: 10.1016/0016-7037(78)90092-3.

Kawabata, H. and N. Takafuji (2005). "Origin of garnet crystals in calc-alkaline volcanic rocks from the Setouchi volcanic belt, Japan". *Mineralogical Magazine* 69.6, pp. 951–971. DOI: 10.1180/0026461056960301.

Konečný, V., J. Lexa, R. Halouzka, L. Dublan, L. Šimon, M. Stolár, A. Nagy, M. Polák, J. Vozár, M. Havrila, et al. (1998a). "Geological map of the region Štiavnické vrchy Mts. and Pohronsk Inovec Mts". *Geological Survey of the Slovak Republic, Bratislava*. [In Slovak with English summary].

Konečný, V., J. Lexa, R. Halouzka, J. Hók, J. Vozár, L. Dublan, A. Nagy, L. Šimon, M. Havrila, J. Ivanička, et al. (1998b). "Explanatory notes to the geological map of Štiavnické vrchy and Pohronsk Inovec mountain ranges (Štiavnica Stratovolcano)". *Geological Survey of Slovak Republic, Bratislava*. [In Slovak with English summary].

Konečný, V., J. Lexa, and V. Hojstričova (1995). "The Central Slovakia neogene volcanic field : a review". *Acta Vulcanologica* 7.2: *Neogene and related magmatism in the Carpatho-Pannonian region*. Ed. by H. Downes and O. Vaselli, pp. 63–78.

Kriegsman, L. M. and B. J. Hensen (1998). "Back reaction between restite and melt: Implications for geothermobarometry and pressure-temperature paths". *Geology* 26.12, p. 1111. DOI: 10.1130/0091-7613(1998)026<1111:brbram>2.3.co;2.

Lackey, J. S., S. Erdmann, J. S. Hark, R. M. Nowak, K. E. Murray, D. B. Clarke, and J. W. Valley (2011). "Tracing garnet origins in granitoid rocks by oxygen isotope analysis: examples from the South Mountain batholith, Nova Scotia". *The Canadian Mineralogist* 49.2, pp. 417–439. DOI: 10.3749/canmin.49.2.417.

Lackey, J. S., G. A. Romero, A.-S. Bouvier, and J. W. Valley (2012). "Dynamic growth of garnet in granitic magmas". *Geology* 40.2, pp. 171–174. DOI: 10.1130/g32349.1.

Le Breton, N. and A. B. Thompson (1988). "Fluid-absent (dehydration) melting of biotite in metapelites in the early stages of crustal anatexis". *Contributions to Mineralogy and Petrology* 99.2, pp. 226–237. DOI: 10.1007/bf00371463.

Leake, B. E., A. R. Woolley, C. Arps, W. Birch, M. Gilbert, J. Grice, E. Hawthorne, A. Kato, H. Kisch, V. Krivovichev, and et al. (1997). "Nomenclature of amphiboles Report of the Subcommittee on Amphiboles of the International Mineralogical Association Commission on New Minerals and Mineral Names". *European Journal of Mineralogy* 9.3, pp. 623–651. DOI: 10.1127/ejm/9/3/0623.

Lee, H. Y. and J. Ganguly (1988). "Equilibrium Compositions of Coexisting Garnet and Orthopyroxene: Experimental Determinations in the System FeO-MgO-Al2O3-SiO2, and Applications". *Journal of Petrology* 29.1, pp. 93–113. DOI: 10.1093/petrology/29.1.93.

Lexa, J. and V. Konečný (1998). "Geodynamic aspects of the Neogene to Quaternary volcanism". *Geodynamic development of the Western Carpathians*. Ed. by M. Rakús. Vol. 219240. Geological Survey of Slovak Republik, Bratislava, pp. 219–240.

López, S. and A. Castro (2001). "Determination of the fluid–absent solidus and supersolidus phase re-

lationships of MORB-derived amphibolites in the range 4–14 kbar". *American Mineralogist* 86.11-12, pp. 1396–1403. doi: 10.2138/am-2001-11-1208.

Miller, C. F., S. M. McDowell, and R. W. Mapes (2003). "Hot and cold granites? Implications of zircon saturation temperatures and preservation of inheritance". *Geology* 31.6, p. 529. doi: 10.1130/0091-7613(2003)031<0529:hacgio>2.0.co;2.

Miller, J. S., J. E. Matzel, C. F. Miller, S. D. Burgess, and R. B. Miller (2007). "Zircon growth and recycling during the assembly of large, composite arc plutons". *Journal of Volcanology and Geothermal Research* 167.1-4, pp. 282–299. doi: 10.1016/j.jvolgeores.2007.04.019.

Miyashiro, A. (1955). "Pyralspite garnets in volcanic rocks". *Journal of the Geological Society of Japan* 61.721, pp. 463–470. doi: https://doi.org/10.5575/geosoc.61.463.

Moecher, D. P., E. J. Essene, and L. M. Anovitz (1988). "Calculation and application of clinopyroxene-garnet-plagioclase-quartz geobarometers". *Contributions to Mineralogy and Petrology* 100.1, pp. 92–106. doi: 10.1007/bf00399441.

Moore, G. and I. S. E. Carmichael (1998). "The hydrous phase equilibria (to 3 kbar) of an andesite and basaltic andesite from western Mexico: constraints on water content and conditions of phenocryst growth". *Contributions to Mineralogy and Petrology* 130.3-4, pp. 304–319. doi: 10.1007/s004100050367.

Moscati, R. J. and C. A. Johnson (2014). "Major element and oxygen isotope geochemistry of vapour-phase garnet from the Topopah Spring Tuff at Yucca Mountain, Nevada, USA". *Mineralogical Magazine* 78.4, pp. 1029–1041. doi: 10.1180/minmag.2014.078.4.14.

Murphy, M. D., R. S. J. Sparks, J. Barclay, M. R. Carroll, and T. S. Brewer (2000). "Remobilization of Andesite Magma by Intrusion of Mafic Magma at the Soufriere Hills Volcano, Montserrat, West Indies". *Journal of Petrology* 41.1, pp. 21–42. doi: 10.1093/petrology/41.1.21.

Myers, J. D. and D. A. Johnston (1996). "Phase Equilibria Constraints on Models of Subduction Zone Magmatism". *Subduction Top to Bottom*. Ed. by G. E. Bebout, D. W. Scholl, S. H. Kirby, and J. P. Platt. American Geophysical Union, pp. 229–249. doi: 10.1029/gm096p0229.

Nakajima, K. and M. Arima (1998). "Melting experiments on hydrous low-K tholeiite: Implications for the genesis of tonalitic crust in the Izu-Bonin - Mariana arc". *The Island Arc* 7.3, pp. 359–373. doi: 10.1111/j.1440-1738.1998.00195.x.

Newton, R. C. and D. Perkins III (1982). "Thermodynamic calibration of geobarometers based on the assemblages garnet-plagioclase-orthopyroxene (clinopyroxene)-quartz". *American Mineralogist* 67.3-4, pp. 203–222.

Nitoi, E., M. Munteanu, S. Marincea, and V. Paraschivoiu (2002). "Magma–enclave interactions in the East Carpathian Subvolcanic Zone, Romania: petrogenetic implications". *Journal of Volcanology and Geothermal Research* 118.1-2, pp. 229–259. doi: 10.1016/s0377-0273(02)00258-5.

Patiño Douce, A. E. (1995). "Experimental generation of hybrid silicic melts by reaction of high-Al basalt with metamorphic rocks". *Journal of Geophysical Research: Solid Earth* 100.B8, pp. 15623–15639. doi: 10.1029/94jb03376.

– (1996). "Effects of pressure and H2O content on the compositions of primary crustal melts". *Earth and Environmental Science Transactions of the Royal Society of Edinburgh* 87.1-2, pp. 11–21. doi: 10.1017/s026359330000643x.

Patiño Douce, A. E. and J. S. Beard (1995). "Dehydration-melting of Biotite Gneiss and Quartz Amphibolite from 3 to 15 kbar". *Journal of Petrology* 36.3, pp. 707–738. doi: 10.1093/petrology/36.3.707.

Perkins, D. and S. J. Chipera (1985). "Garnet-orthopyroxene-plagioclase-quartz barometry: refinement and application to the English River subprovince and the Minnesota River valley". *Contributions to Mineralogy and Petrology* 89.1, pp. 69–80. doi: 10.1007/bf01177592.

Pichavant, M., J.-M. Montel, and L. R. Richard (1992). "Apatite solubility in peraluminous liquids: Experimental data and an extension of the Harrison-Watson model". *Geochimica et Cosmochimica Acta* 56.10, pp. 3855–3861. doi: 10.1016/0016-7037(92)90178-l.

Pickering, J. M. and D. A. Johnston (1998). "Fluid-Absent Melting Behavior of a Two-Mica Metapelite: Experimental Constraints on the Origin of Black Hills Granite". *Journal of Petrology* 39.10, pp. 1787–1804. doi: 10.1093/petroj/39.10.1787.

Popov, V. S. (1983). "Garnet composition as an indicator of the origin of calc-alkaline igneous rocks". *International Geology Review* 25.4, pp. 395–406. doi: 10.1080/00206818309466716.

Pownceby, M. I., V. J. Wall, and H. S. C. O'Neill (1991). "An experimental study of the effect of Ca upon garnet-ilmenite Fe-Mn exchange equilibria". *American Mineralogist* 76.9-10, pp. 1580–1588.

Rapp, R. P. and E. B. Watson (1995). "Dehydration Melting of Metabasalt at 8-32 kbar: Implications for Continental Growth and Crust-Mantle Recycling". *Journal of Petrology* 36.4, pp. 891–931. doi: 10.1093/petrology/36.4.891.

Ridolfi, F., A. Renzulli, and M. Puerini (2010). "Stability and chemical equilibrium of amphibole in calc-alkaline magmas: an overview, new thermobarometric formulations and application to subduction-related volcanoes". *Contributions to Mineralogy and Petrology* 160.1, pp. 45–66. doi: 10.1007/s00410-009-0465-7.

Rottier, B., A. Audétat, P. Koděra, and J. Lexa (2019). "Origin and Evolution of Magmas in the Porphyry Au-mineralized Javorie Volcano (Central Slovakia): Evidence from Thermobarometry, Melt Inclusions and Sulfide Inclusions". *Journal of Petrology* 60.12, pp. 2449–2482. DOI: 10.1093/petrology/egaa014.

Rutherford, M. J. and P. M. Hill (1993). "Magma ascent rates from amphibole breakdown: An experimental study applied to the 1980-1986 Mount St. Helens eruptions". *Journal of Geophysical Research: Solid Earth* 98.B11, pp. 19667–19685. DOI: 10.1029/93jb01613.

Schmidt, M. W. (1992). "Amphibole composition in tonalite as a function of pressure: an experimental calibration of the Al-in-hornblende barometer". *Contributions to Mineralogy and Petrology* 110.2-3, pp. 304–310. DOI: 10.1007/bf00310745.

Schwandt, C. S. and G. A. McKay (2006). "Minor- and trace-element sector zoning in synthetic enstatite". *American Mineralogist* 91.10, pp. 1607–1615. DOI: 10.2138/am.2006.2093.

Seghedi, I. (2004). "Neogene–Quaternary magmatism and geodynamics in the Carpathian–Pannonian region: a synthesis". *Lithos* 72.3-4, pp. 117–146. DOI: 10.1016/j.lithos.2003.08.006.

– (2010). "Miocene-recent magmatism and geodynamic processes in the Carpathian-Pannonian region-relations with Balkan and Aegean areas". *Geologica Balcanica* 39.1/2, pp. 9–11.

Seifert, F. and J. Schumacher (1986). "Cordierite-spinel-quartz assemblages: A potential geobarometer". *Bulletin of the Geological Society of Finland* 58.1, pp. 95–108. DOI: 10.17741/bgsf/58.1.007.

Sen, S. K. and A. Bhattacharya (1984). "An orthopyroxene-garnet thermometer and its application to the Madras charnockites". *Contributions to Mineralogy and Petrology* 88.1-2, pp. 64–71. DOI: 10.1007/bf00371412.

Skjerlie, K. P. and A. D. Johnston (1993). "Fluid-Absent Melting Behavior of an F-Rich Tonalitic Gneiss at Mid-Crustal Pressures: Implications for the Generation of Anorogenic Granites". *Journal of Petrology* 34.4, pp. 785–815. DOI: 10.1093/petrology/34.4.785.

– (1996). "Vapour-Absent Melting from 10 to 20 kbar of Crustal Rocks that Contain Multiple Hydrous Phases: Implications for Anatexis in the Deep to Very Deep Continental Crust and Active Continental Margins". *Journal of Petrology* 37.3, pp. 661–691. DOI: 10.1093/petrology/37.3.661.

Skjerlie, K. P., A. E. Patiño Douce, and A. D. Johnston (1993). "Fluid absent melting of a layered crustal protolith: implications for the generation of anatectic granites". *Contributions to Mineralogy and Petrology* 114.3, pp. 365–378. DOI: 10.1007/bf01046539.

Spear, F. S. and M. J. Kohn (1999). *Program Thermobarometry (GTB, version 2.1)*. Tech. rep. [GTB program manual].

Stevens, G., J. D. Clemens, and G. T. R. Droop (1997). "Melt production during granulite-facies anatexis: experimental data from "primitive" metasedimentary protoliths". *Contributions to Mineralogy and Petrology* 128.4, pp. 352–370. DOI: 10.1007/s004100050314.

Taylor, J. and G. Stevens (2010). "Selective entrainment of peritectic garnet into S-type granitic magmas: Evidence from Archaean mid-crustal anatectites". *Lithos* 120.3-4, pp. 277–292. DOI: 10.1016/j.lithos.2010.08.015.

Thompson, A. B. (1982). "Dehydration melting of pelitic rocks and the generation of H 2 O-undersaturated granitic liquids". *American Journal of Science* 282.10, pp. 1567–1595. DOI: 10.2475/ajs.282.10.1567.

Tindle, A. and P. Webb (1994). "Probe-AMPH—A spreadsheet program to classify microprobe-derived amphibole analyses". *Computers & Geosciences* 20.7-8, pp. 1201–1228. DOI: 10.1016/0098-3004(94)90071-x.

Ulmer, P., R. Kaegi, and O. Müntener (2018). "Experimentally Derived Intermediate to Silica-rich Arc Magmas by Fractional and Equilibrium Crystallization at 1·0GPa: an Evaluation of Phase Relationships, Compositions, Liquid Lines of Descent and Oxygen Fugacity". *Journal of Petrology* 59.1, pp. 11–58. DOI: 10.1093/petrology/egy017.

Venezky, D. Y. and M. J. Rutherford (1997). "Preeruption conditions and timing of dacite-andesite magma mixing in the 2.2 ka eruption at Mount Rainier". *Journal of Geophysical Research: Solid Earth* 102.B9, pp. 20069–20086. DOI: 10.1029/97jb01590.

Vielzeuf, D. and J. R. Holloway (1988). "Experimental determination of the fluid-absent melting relations in the pelitic system". *Contributions to Mineralogy and Petrology* 98.3, pp. 257–276. DOI: 10.1007/bf00375178.

Vielzeuf, D. and J. M. Montel (1994). "Partial melting of metagreywackes. Part I. Fluid-absent experiments and phase relationships". *Contributions to Mineralogy and Petrology* 117.4, pp. 375–393. DOI: 10.1007/bf00307272.

Vielzeuf, D. and M. W. Schmidt (2001). "Melting relations in hydrous systems revisited: application to metapelites, metagreywackes and metabasalts". *Contributions to Mineralogy and Petrology* 141.3, pp. 251–267. DOI: 10.1007/s004100100237.

Villaros, A., G. Stevens, and I. S. Buick (2009). "Tracking S-type granite from source to emplacement: Clues from garnet in the Cape Granite Suite". *Lithos* 112.3-4, pp. 217–235. DOI: 10.1016/j.lithos.2009.02.011.

Watson, E. B. (1979). "Zircon saturation in felsic liquids: Experimental results and applications to trace element geochemistry". *Contributions to Mineralogy and Petrology* 70.4, pp. 407–419. DOI: 10.1007/bf00371047.

Watson, E. B. and T. M. Harrison (1983). "Zircon saturation revisited: temperature and composition effects in a variety of crustal magma types". *Earth and Planetary Science Letters* 64.2, pp. 295–304. doi: 10.1016/0012-821x(83)90211-x.

Whitney, D. L. and B. W. Evans (2010). "Abbreviations for names of rock-forming minerals". *American Mineralogist* 95.1, pp. 185–187. doi: 10.2138/am.2010.3371.

Winther, K. T. (1991). "Experimental melting of hydrous low-K tholeiite: evidence on the origin of Archean cratons". *Bulletin of the Geological Society of Denmark* 39, pp. 213–228.

Wolf, M. B. and P. J. Wyllie (1993). "Garnet Growth during Amphibolite Anatexis: Implications of a Garnetiferous Restite". *The Journal of Geology* 101.3, pp. 357–373. doi: 10.1086/648229.

Yardley, B. W. D. and J. W. Valley (1997). "The petrologic case for a dry lower crust". *Journal of Geophysical Research: Solid Earth* 102.B6, pp. 12173–12185. doi: 10.1029/97jb00508.

Zeck, H. P. (1970). "An erupted migmatite from Cerro del Hoyazo, SE Spain". *Contributions to Mineralogy and Petrology* 26.3, pp. 225–246. doi: 10.1007/bf00373202.

Zhang, C., F. Holtz, J. Koepke, P. E. Wolff, C. Ma, and J. H. Bédard (2013). "Constraints from experimental melting of amphibolite on the depth of formation of garnet-rich restites, and implications for models of Early Archean crustal growth". *Precambrian Research* 231, pp. 206–217. doi: 10.1016/j.precamres.2013.03.004.